The FASEB Journal
The Journal of the Federation of American Societies for Experimental Biology
All Articles | Submit | Subscribe | What's New | RSS

FASEB J. 2019 Nov; 33(11): 12853–12872.

Published online 2019 Sep 13. doi: 10.1096/fj.201900057R: 10.1096/fj.201900057R

PMCID: PMC6902701

PMID: 31518158

Ambient and supplemental magnetic fields promote myogenesis *via* a TRPC1-mitochondrial axis: evidence of a magnetic mitohormetic mechanism

Jasmine Lye Yee Yap,[*†,1] Yee Kit Tai,[*†,1] Jürg Fröhlich,[*‡] Charlene Hui Hua Fong,[*†] Jocelyn Naixin Yin,[*†] Zi Ling Foo,[*†] Sharanya Ramanan,[*†] Christian Beyer,[‡§] Shi Jie Toh,[*†] Marco Casarosa,[¶] Narendra Bharathy,[‖#] Monica Palanichamy Kala,[‖] Marcel Egli,[**] Reshma Taneja,[‖] Chuen Neng Lee,[*††] and Alfredo Franco-Obregón[*†‖††,2]

[1]These authors contributed equally to this work.

[2]Correspondence: National University Singapore, National University Hospital, NUHS Tower Block, Level 8, 1E Kent Ridge Rd., Singapore 119228, Singapore., E-mail: gs.ude.sun@farus

Received 2019 Jan 8; Accepted 2019 Aug 12.

Skeletal muscle status determines whole-body metabolism. Exercise metabolically activates muscle that, in turn, stimulates muscle to produce and release myokines that benefit systemic metabolism and cardiovascular function (1, 2). Consequently, physical inactivity and the resultant loss of skeletal muscle is a major determinant of morbidity in aging populations.

Muscle physical and metabolic adaptations largely rely on calcium acquisition that is partially satisfied by mechanically gated cation channels (3). Diverse transient receptor potential (TRP) channel family members have been implicated in numerous forms of cellular mechanosensation (4), and evidence exists that the mechanosensitive currents detected in muscle (5) correspond to a signaling complex containing TRPC1 (6). Accordingly, TRPC1 has been implicated in load-dependent oxidative muscle development (7, 8). Exercise promotes oxidative muscle development, whereas inactivity results in the atrophy of oxidative muscle. Oxidative fibers exhibit higher resting calcium levels that diminish upon mechanical unloading and precede a reversal in oxidative character (3). TRPC1 expression is highest in oxidative muscle fibers (9) and wanes with disuse (8). Accordingly, silencing

TRPC1 expression results in oxidative muscle loss (8). TRPC1-mediated calcium entry coactivates calcineurin and the nuclear factor of activated T cells (NFAT) (8, 10) that, in turn, sustains TRPC1 transcription (8, 11). In a parallel manner, calcineurin/NFAT and TRPC1 levels decrease upon mechanical unloading and revert upon reloading (8, 12), mirroring decreases and increases of oxidative muscle expression, respectively. Ample evidence thus supports roles for TRPC1 and calcineurin/NFAT in calcium-sensitive oxidative muscle development.

Mitochondrial adaptations are central to muscular and systemic metabolic homeostasis and are largely reliant on the activity of the transcriptional coactivator, peroxisome proliferator–activated receptor-γ coactivator-1α (PGC-1α) (1, 2). PGC-1α is a major determinant in oxidative muscle development and maintenance because of its regulatory role over mitochondriogenesis that is necessary to sustain the heightened mitochondrial oxidative respiration of said muscle (13). In alignment with the calcium/calcineurin dependency of oxidative muscle development, PGC-1α enhancement of oxidative muscle development is enhanced by calcium/calcineurin (13). A calcium-mitochondrial interplay is thus necessary for oxidative muscle development.

Life evolved in a biosphere characterized by a standing magnetic field. It thus stands to reason that magnetic fields should impact development, an assumption increasingly supported in the scientific literature. Nonetheless, the cellular transduction apparatuses responsible for converting magnetic fields into biochemical and genetic cellular responses and how they may be influenced by environmental factors remain largely unexplored, altering the efficacy of detected responses and causing discordance in the field (14). Previous studies have shown that pulsed magnetic fields (PEMFs) are capable of regulating myoblast calcium homeostasis, mitochondrial respiration, resistance to oxidative stress (15), and expansion (16). Here we provide evidence that TRPC1 is both necessary and sufficient for magnetic fields, both ambient and supplemental, to promote both mitochondriogenesis and myogenesis (**Fig. 1**). Noteworthy, the conventional use of aminoglycoside antibiotics, because of their propensity to block TRPC1 (17), has likely masked the potential therapeutic value of magnetic fields in previous *in vitro* studies. Finally, we provide evidence for a host of other commonly encountered circumstances that may have prevented previous investigators from detecting magnetically induced developmental responses and contributed to slowing progress in this important area of study.

MATERIALS AND METHODS

Cell studies and analysis

Cell culture and pharmacology

C2C12 mouse skeletal myoblasts were obtained from American Type Culture Collection (LGC Standards, Teddington, United Kingdom) and cultured in growth medium (GM) consisting of DMEM (Thermo Fisher Scientific, Waltham, MA, USA) and supplemented with 10% fetal bovine serum (FBS; Biowest, Nuaillé, France) and 2 mM L-glutamine (Thermo Fisher Scientific) in a humidified incubator at 37°C in 5% CO_2. Cells were

passaged every 48 h to maintain them below 40% confluence at all times. Myoblasts were seeded into tissue culture dishes/flasks at 3000 cells/cm^2. Allowing myoblasts to become senescent by overpassaging at high confluence greatly increased the incidence of nonrespondent cultures. Analysis was hence restricted to low passage (<6) myoblast cultures that were never allowed to exceed 50% confluence prior to exposure to PEMFs. Moreover, the level of FBS supplementation, as it modulates time to reach confluence (growth rate), influences sensitivity to PEMFs; with few exceptions, FBS was kept at 10% for all experiments. Penicillin and streptomycin were excluded from the culturing medium as the aminoglycoside antibiotics block TRPC channels (17) and, accordingly, negate the effects of the fields over myogenesis. When these criteria were adhered to, cells responded characteristically to PEMFs. Proliferation was ascertained 24 h after exposure to PEMFs unless otherwise indicated in the figure legends or elsewhere.

The differentiation of myoblasts was induced with a change in medium serum composition from 10% FBS to 2% horse serum (HyClone; Thermo Fisher Scientific) at 24 h after plating at 6000 cells/cm^2. For the determination of fusion index, cells were fixed with 70% ethanol, 37% formaldehyde, and glacial acetic acid in a ratio of 20:2:1 and hematoxylin and eosin staining was performed for the visualizing of the cytoplasm and nuclei. A series of 10 images with ×10 magnification was taken for each sample, and myonuclei in myoblasts and myotubes were quantified using ImageJ [Cell Counter plugin; National Institutes of Health (NIH), Bethesda, MD, USA]. Fusion analysis was conducted 4–6 d postinduction.

2-Aminoethoxydiphenylborate (2-APB) and ruthenium red (MilliporeSigma, Burlington, MA, USA) were administered to cells 15–30 min before exposure to PEMFs at a working concentration of 10 μM. Tetrodotoxin (TTX; Alomone Labs, Jerusalem, Israel) was administered 10 min prior to PEMF exposure at a working concentration of 1 μM. PEMF antagonism of TRPC1 by aminoglycoside antibiotics was examined using 1% penicillin/streptomycin (PS), which is composed of 100 U/ml penicillin (~67 mg/ml) and 100 μg/ml streptomycin (Thermo Fisher Scientific) or the pure aminoglycosides antibiotics streptomycin (S9137; MilliporeSigma) or neomycin (N6386; MilliporeSigma) at the concentrations indicated and were applied immediately before exposure. Cyclosporin A (CsA; MilliporeSigma) was administered to cells 10 min before exposure to PEMFs at a working concentration of 80 μM. Culture media containing either 2-APB, CsA, or aminoglycoside antibiotics were summarily replaced after PEMF exposure with medium obtained from nonstimulated age-matched sister cultures.

DNA content measurement

Cells were seeded at 1500 cells/well in a 96-well plate in replicates of 4. Twenty-four hours post-PEMF, cells were incubated with 100 ul of CyQuant direct reagent (Thermo Fisher Scientific) for 1 h before analysis at 480/535 nm using a Cytation5 (BioTek Instruments, Winooski, VT, USA) plate reader.

Calcium imaging

In preparation for measuring changes in intracellular calcium in response to PEMF treatment with flow cytometry, myoblasts (50,000 cells) were spun down (1000 *g*; 5 min), resuspended in 2 ml of PBS, and loaded with 20 µl Calcium Green-1, AM (50 µg in 100 µl DMSO; Molecular Probes, Eugene, OR, USA) for 30 min at 37°C in the dark. Following incubation, cells were washed once, resuspended in 500 µl PBS, and placed on ice before registry in a BD fluorescence-activated cell sorting (FACS) Aria Flow Cytometer (FL1 channel; BD Biosciences, San Jose, CA, USA).

For plate reading assessment of intracellular calcium, myoblasts were plated into 96-well black-bottom polystyrene plates (Thermo Fisher Scientific) at 10,000 cells/wells. Cultures were washed once with PBS and supplied with 100 µl GM to which Calcium Green-1, AM (50 µg in 100 µl DMSO) had been added at dilution of 1:1000. Myoblasts cultures were then incubated in a standard tissue culture incubator for 30 min for the loading of Calcium Green-1, AM and followed by addition of 100 µl of PS and 2-APB in GM to a working concentration of 1% and 100 µM, respectively. PEMF exposure (10 min) was given and then calcium measurement was conducted using a Infinite 200 Pro Plate Reader (Tecan, Zurich, Switzerland) with excitation wavelength and emission wavelengths set to 500 and 535 nm, respectively, and bandwidth excitation and emission wavelengths set to 9 and 20 nm, respectively.

Western blots

Total protein extraction was carried out using RIPA lysis buffer containing 50 mM NaCl, 1 mM EDTA, 50 mM Tris-HCl, 1% Triton X-100, 0.05% SDS, 1× protease inhibitor (Thermo Fisher Scientific), and 0.1% sodium deoxycholate (MilliporeSigma). Lysates were collected using a cell scraper and incubated at 4°C for 30 min before being spun at 12,000 rpm for 15 min at 4°C. Protein samples with 1× loading dye were boiled at 95°C, resolved on SDS-PAGE, transferred to PVDF membrane (Thermo Fisher Scientific), blocked with 5% low-fat milk, and probed with anti–P300/CBP-associated factor (PCAF; Santa Cruz Biotechnology, Dallas, TX, USA), anti-myoblast determination protein 1 (MyoD; Santa Cruz Biotechnology), and anti–β-actin (MilliporeSigma) antibodies. For TRPC1 and TRPM7 silencing experiments, membranes were probed with anti-TRPC1 (Santa Cruz Biotechnology), anti-TRPM7 (Alomone Labs), anti–glyceraldehyde 3-phosphate dehydrogenase (GAPDH), and anti-cyclin D1 (Proteintech, Rosemont, IL, USA) antibodies. Other antibodies used were anti-TRPC3 (Santa Cruz Biotechnology), and anti-TRPC6, anti-TRPV1, and anti-TRPV4 were from Alomone Labs. Anti–Mcl-1, anti-Bcl-xL, anti-Caspase 9, anti-Caspase 7 anti–Caspase-3 were from Cell Signaling Technology (Danvers, MA, USA). All anti-Caspase antibodies detect full length as well as cleaved forms of the proteins. For histone protein extract, 1× Laemmli buffer containing 62.5 mM Tris, pH 6.8, 10% glycerol, 2% SDS, and 1× protease inhibitor (Thermo Fisher Scientific) was added to the cells and lysates collected. Samples were heated for 10 min at 95°C then allowed to set to room temperature. Samples were briefly sonicated and heated for 5 min at 95°C in 5× loading buffer (Bio-Rad, Hercules, CA, USA) before running on SDS-PAGE. Proteins were transferred to PVDF membranes and immunoblotted with anti-H3K9ac and anti-H3 antibodies (Abcam, Cambridge, United Kingdom).

For subcellular fractionation for the analysis of the nuclear-cytoplasmic partitioning of NFATC1 and NFATC3 cells were lysed in hypotonic buffer consisting of 250 mM sucrose, 20 mM HEPES (pH 7.4), 10 mM KCl, 1.5 mM $MgCl_2$, 1 mM EDTA, 1 mM DTT, and 1× protease inhibitor. Lysates were centrifuged at 700 *g* for 5 min, and the nuclear pellets were lysed in buffer containing 50 mM Tris-HCl (pH 8), 150 mM NaCl, 1% Triton X-100, 1 mM EDTA, 1 mM DTT and 1× protease inhibitor. Proteins that were resolved on SDS-PAGE gels were transferred onto PVDF membranes and probed with anti-NFATC1 and anti-NFATC3 antibodies (Santa Cruz Biotechnology) and anti–lamin B1 (Proteintech).

Quantitative RT-PCR

Total RNA was harvested from C2C12 myoblasts at selected time points using Trizol reagent (Thermo Fisher Scientific) and 0.5 µg of total RNA was reverse transcribed using iScript cDNA Synthesis Kit (Bio-Rad). A total of 2 ng RNA was converted to cDNA template for quantitative PCR reactions. Quantification of mRNA expression was performed using Taqman Gene Expression Assays (Thermo Fisher Scientific) and SSoAdvanced Universal SYBR Green (Bio-Rad) on the CFX Touch Real-Time PCR Detection System (Bio-Rad). Relative mRNA expression was determined by the $2^{-\Delta\Delta Ct}$ method, normalized to β-2 microglobulin (B2M) mRNA levels and using the following primer sets (**Table 1**).

TRP channel silencing

Dicer-substrate interfering RNAs

Silencing of TRPC1 was performed using 2 independent dicer-substrate interfering RNAs (dsiRNA) against TRPC1 (NM_011643). The 2 dsiRNAs target the coding sequence of exon 3 (Dsi1) and untranslated coding sequence of exon 13 (Dsi2). The silencing of TRPM7 (NM_021450) was achieved by targeting the 3′ UTR of TRPM7. The dsiRNAs were acquired from Integrated DNA Technologies (Coralville, IA, USA). Transfection of dsiRNAs at 10 nM was carried out using Lipofectamine 2000 (Thermo Fisher Scientific) according to the manufacturer's instructions. Briefly, cells were incubated with transfection mixture of Lipofectamine and dsiRNA for 24 h prior to PEMF exposure, followed by cell counting and Western blot analysis 24 h later.

Clustered regularly interspaced short palindromic repeats/ CRISPR-associated protein 9 plasmid design, construction, and transfection into C2C12 cells

For the selection of candidate single-guide RNAs (sgRNAs) for mouse TRPC1 genome editing, the integral genomic sequence from the first exon of *TRPC1* (NC_000075.6) was submitted to the clustered regularly interspaced short palindromic repeats (CRISPR) design tool (*http://crispr.mit.edu*). The sgRNAs were designed to flank the start codon of TRPC1 found in exon 1. Candidate sgRNAs of 20 nt length, CCACTCTGTCGTCCCCGGAC and TTCTTGCTGGCGTGCGACAA, were cloned into PX458 (pSpCas9-P2A-GFP) and PX459 (pSpCas9-P2A-Puro), respectively. Plasmids were digested with *Bbs*I, and then the sgRNA oligonucleotides were cloned into the plasmids according to previously described protocols (18). Sequencing verified plasmids were transfected into C2C12 myoblasts using

Lipofectamine 3000 (Thermo Fisher Scientific) (Supplemental Fig. S9). Transiently transfected myoblasts were single-cell green fluorescent protein–sorted (SuperMACSTM II Separator) and subsequently selected using puromycin (Santa Cruz Biotechnology). Genomic DNA from single-cell colonies was genotyped using PCR with the following primer pairs: forward 5′-GGATGACGTGAGGAGAAAGCC-3′ and reverse 5′-CAGAGGTGGGAATAGCCGC-3′. Genomic DNA from single-cell colonies were sequence-verified for deletion of exon 1 (Supplemental data) as well as analyzed for TRPC1 protein expression with Western blot analysis. Despite the successful deletion of the standard initiation start codon in exon 1 of the TRPC1 gene, residual TRPC1 protein expression that was observed can be explained by the existence of several lower efficiency alternative 5′ upstream non-AUG translational start sites spared by our procedure (19). Regardless, our TRPC1 knockdowns demonstrated reduced magnetic sensitivity.

Cell cycle analysis

Cell cycle analysis was performed as previously described (6, 12). Following random positioning machine (RPM) treatment (below), cells were fixed and stored at −20°C in 70% ice-cold ethanol for 12–18 h prior to staining. Cell cycle was analyzed based on DNA content using a propidium iodide/RNase Staining Kit (BD Biosciences) by flow cytometry.

Quantification of mitochondrial DNA

C2C12 myoblasts were seeded into T-75 tissue culture flasks at 3000 cells/cm^2. Total cellular DNA was extracted 24 h post-PEMF using GF-1 Tissue Blood Combi DNA Extraction Kit (GF-BT-100; Vivantis Technologies, Selangor, Malaysia), according to the manufacturer's instructions. PCR was performed for mitochondrial DNA-encoded cytochrome *c* oxidase subunit II (COXII; forward 5′-GCCGACTAAATCAAGCAACA-3′, reverse 5′-CAATGGGCATAAAGCTATGG-3′), mitochondrial-encoded 16S rRNA (forward 5′-CCGCAAGGGAAAGATGAAAGAC-3′, reverse 5′-TCGTTTGGTTTCGGGGTTTC-3′), and nucleus-encoded GAPDH (forward 5′-TGA CGTGCCGCCTGGAGA AA-3′, reverse 5′-AGTGTAGCCCAAGATGCCCTTCAG-3′) genes using Rediant 2× PCR Master Mix (BIO-5185-200, first Base; Alkali Scientific; Fort Lauderdale, FL, USA). The specificity and quantity of the amplified PCR products were confirmed by sample separation using 1.7% DNA agarose gel. The gel electrophoresis images were captured using ChemiDoc Touch Imaging System (Bio-Rad), and the mitochondrial DNA to nuclear DNA ratio was determined using Image Studio v.5.2.5 (Li-Cor Biosciences, Lincoln, NE, USA).

Metabolic flux and reactive oxygen species analysis

C2C12 myoblasts were seeded into Agilent Seahorse XFe24 plates in GM at a density of 20,000 or 30,000 cells/well for 20 h before PEMF exposure. Following PEMF exposure (10 min), myoblasts were allowed to stabilize for 2 h in a standard humidified incubator at 37°C and 5% CO_2. For the assessment of contribution from TRPC1, SKF-96365 (50 μM; MilliporeSigma) was added to the GM of myoblasts cultures 10 min prior to PEMF exposure and replaced with GM from age-matched sister cultures immediately afterward. In preparation for mitochondrial assessment, the GM was replaced with XF Base medium

(Agilent Technologies, Santa Clara, CA, USA) consisting of 10 mM glucose, 1 mM sodium pyruvate, and 2 mM glutamine (pH 7.4) and equilibrated in a non-CO_2 environment at 37°C for 60 min, as per the manufacturer's suggested protocol. Cellular respiratory capacity was assayed using the XF Cell Mito Stress Test Kit (Agilent Technologies). Briefly, the assay consists of repeated cycles of 3-min mix, 2-min wait, and 3-min measurement cycles for baseline and after each injection of oligomycin (1 μM), carbonyl cyanide 4-(trifluoromethoxy) phenylhydrazone (FCCP, 1 μM), and rotenone + antimycin A (0.5 μM). Oxygen consumption rate (OCR) and extracellular acidification rate (ECAR), reflecting mitochondrial respiration and glycolysis, respectively, were measured simultaneously during each measurement period. Data analysis was done using Seahorse Wave Desktop Software (Agilent Technologies).

For reactice oxygen species (ROS) analysis by flow cytometry (Fig. 6*A, B*), CellROX Orange Reagent (Thermo Fisher Scientific) was added to C2C12 myoblasts in suspension at a density of 250,000 cells/ml to a final concentration of 750 nM just prior to standard PEMF exposure. Cells were then incubated with the dye for an additional 1 h at 37°C before analysis using a FACS BD LSRFortessaTM flow cytometer (absorption/emission maxima of ~545/565 nm; BD Biosciences) as per the manufacturer's instructions. A measure of 400 μM *tert*-butyl hydroperoxide (MilliporeSigma) was used as a positive control. Data analysis was performed using FACSDiva v.6.2, Summit v.4.3, and Prism v.5.0 (NIH).

For ROS analysis *via* plate reading, cells were seeded at 5000 cells/well in 96-well plates for 24 h. Prior to standard PEMF exposure, cells were administered CellRox Orange Reagent (Thermo Fisher Scientific) without or with 1% PS or SFK96365 (50 μM) for 10 min. Readings were made at 545/565 nm using a Cytation 5 plate reader (Biotek Instruments). For cell proliferation analysis, 3000 cells/cm^2 were seeded in 6-well plates for 24 h. *N*-Acetylcysteine (5 mM; Santa Cruz Biotechnology) was added to the GM 10 min prior to standard PEMF exposure and was replaced with conditioned GM from age-matched sister cultures that had not been exposed to PEMFs immediately thereafter. Cells were enumerated using Trypan Blue 24 h later.

ATP detection

C2C12 myoblasts were seeded into clear 96-well plates at 5000 cells/well and exposed to PEMFs after 24 h of growth. Cells were harvested 30 min after exposure using Cayman Chemical ATP Detection Assay Kit-Luminescence (700410; Ann Arbor, MI, USA), according to the manufacturer's instructions. The samples were diluted 40 times in 1× ATP Sample Buffer before loading them into a white opaque 96-well plate. The ATP concentration was determined by luminescence reading using Cytation 5 Cell Imaging Multi-Mode Reader and its respective Gen5 software for analysis (BioTek Instruments). TRPC-dependent ATP production was obtained by subtracting ATP signal in the presence of SKF-96365 (50 μM) from PEMF-induced signals at 0 and 1.5 mT.

BrdU flow cytometric analysis

BrdU staining was performed according to BrdU staining kit for flow cytometry FITC (Thermo Fisher Scientific). Briefly, C2C12 myoblasts were seeded at 6000 cells/cm^2 into 6-well plates and allowed to grow for 40 h. Immediately prior to PEMF exposure as described next, the medium was changed to fresh medium containing BrdU. Cells were allowed to incorporate BrdU labeling after PEMF exposure for 6 h before fixation, DNase I treatment and intracellular staining with anti-BrdU conjugated to FITC. Cell washes between steps were done using Flow Cytometry Staining Buffer (Thermo Fisher Scientific) at 400 *g* for 5 min. Resuspended cells were subjected to flow analysis using FACS BD LSR Fortessa (BD Biosciences).

Electromagnetic and simulated microgravity exposure systems

PEMF device

The PEMF device used in this study has been previously described (20, 21). Briefly, the device produces spatially homogeneous, time-varying magnetic fields, consisting of barrages of 20 × 150 μs on and off pulses for 6 ms repeated at a frequency of 15 Hz. The magnetic flux density rose to predetermined maximal level within ∼50 μs (∼17 T/s) when driving field amplitudes between 0.5 and 3 mT. Unless explicitly noted, all samples were exposed once for 10 min. All PEMF-treated samples were compared with time-matched control samples (0 mT) that were manipulated in exactly the same way as experimental samples, including placement into the PEMF-generating apparatus for the designated time, except that the apparatus was not set to generate a magnetic field.

μ-Metal shielding of magnetic fields

After in-house designing the fabrication of a μ-metal housing to simultaneously shield 2 standard tissue culture plates from exogenous magnetic fields was contracted from Amuneal Manufacturing (Philadelphia, PA, USA).

Mechanical vibration

This inherent vibration of the PEMF coil system was measured with a vibration transducer BU-21771-000 (Knowles Electronics, Itasca, IL, USA) in a frequency range of 50–6000 Hz. Culture dishes of C2C12 myoblasts were then stimulated with a mechanical signal mimicking the vibration caused by the PEMF exposure system with a TV50018 Shaker System (Tira, Schaulkau, Germany).

Live cell imaging

Live cell imaging was conducted with a CytoSmart 2 Lux 10X System (Lonza Group, Basel, Switzerland) placed within a Forma Steri-Cycle i160 (Thermo Fisher Scientific) standard tissue culture incubator at 37°C in 5% CO_2 and was commenced within 20 min of PEMF exposure. Timelapse videos were downloaded *via* the CytoSmart Connect Cloud as .avi files.

Simulation of microgravity

Simulated microgravity was achieved with an RPM as previously described (12). The RPM was kept in a temperature-controlled room at 37°C. The calculated gravity exerted upon cells on the RPM was below 0.02 *g*. Cells were seeded 15 h prior to the start of the RPM experiment at 8000 cells/cm^2. At 15 h, some samples were incubated with 5 mM $CaCl_2$ for 10 min, washed twice with PBS, given aged-matched GM, and placed onto the RPM. Other samples were exposed to PEMFs at 37°C (0.5 or 1.5 mT) for 10 min before being placed onto the RPM. Samples were fixed after 2 h of growth in micrograms for cell cycle analysis.

Statistical analyses

For the analysis of *in vitro* experiments involving more than 1 experimental condition, each experimental condition was directly compared with a unique control scenario treated identically except for the experimental intervention. For continuous data sets comparing an experimental condition against its respective control, we utilized a 2-tailed Student's *t* test to determine statistical significance. Compared are the mean values of individual experimental mean values each generated a minimum of biological triplicates, unless otherwise stated in the figure legend. For the analysis of distribution frequencies of nuclei within myotubes with a 2 × 3 contingency table, with the rows representing control or PEMF and columns depicting the distribution of nuclei: <4, 5–8, >9 (Fig. 3*H*). For these data sets, a χ^2 test was performed. Statistical significance for all data was set at $P < 0.05$ or $P < 0.01$. All data are presented as means ± SD, unless specified otherwise.

RESULTS

PEMFs stimulate *in vitro* myogenesis

Brief exposure (10 min) of C2C12 myoblasts to PEMFs (Supplemental Fig. S1*A*) augmented cytosolic calcium levels [intracellular [Ca^{2+}] concentration ($[Ca^{2+}]_i$), blue] relative to unexposed myoblasts (red; **Fig. 2*A***). The PEMF-induced rise could be prevented by 2-APB (10 μM; Fig. 2*B*), implicating the involvement of TRPC channels (22) in the early stages of myogenesis while excluding that of voltage-gated calcium channels (6). Moreover, 2-APB lowered $[Ca^{2+}]_i$ to a common baseline whether in PEMF-stimulated (gray) or control (blue gray) myoblasts, indicating that TRP channels are instrumental in establishing resting $[Ca^{2+}]_i$. The red and blue shaded regions depict increments in $[Ca^{2+}]_i$ at rest and following magnetic exposure. These results indicate that the gating mechanism of TRP channels is activated at ambient thermal energy (k_BT) and is reinforced by magnetism.

From here onward, all data relating to PEMF exposures between 1 and 1.5 mT at 24 and 48 h will be depicted in blue and black, respectively, and their correspondent control scenarios (0 mT) in red. Pale blue and hatched conditions will indicate PEMF amplitudes other than 1–1.5 mT (off window) and pharmacological or environmental interventions upon these conditions, respectively. Green will denote auxiliary interventions.

TRPC1-mediated calcium entry supports the proliferation of myoblasts (6, 12). Accordingly, the proliferation of myoblasts was enhanced by 10 min exposure to PEMFs (Fig. 2*C*, dark blue) and could be prevented by both CsA (inset, calcineurin/NFAT inhibitor) and 2-APB

(Fig. 2*C*, hatched), confirming the involvement of TRPC1 and associated calcineurin/NFAT-signaling cascades (8–11). Kinetically, PEMF exposure accelerated the onset and magnitude of early growth expansion (Supplemental Fig. S2 and Supplemental Videos S1*A, B*). The greatest proliferative enhancement was obtained with 10 min exposures (Fig. 2*C*) to PEMFs at an amplitude range between 1 and 1.5 mT (Fig. 2*D*), delimiting a magnetic efficacy window wherein myoblasts are most responsive to supplemental magnetic fields (Supplemental Fig. S3). Differentiation was enhanced (Fig. 2*E–I*) by the same exposure paradigm promoting proliferation (Fig. 2*D*) with similar sensitivity to CsA (Fig. 2*I*).

In vitro, TRPC1 expression is initially high and recedes after 48 h, whereas TRPM7 expression increases after 48 h, coinciding with cell cycle withdrawal (6) (see also Supplemental Fig. S4). The early expression pattern of TRPC1 agrees with reports of it playing a role in satisfying the calcium requirement for myoblast expansion (23). We compared the PEMF responses of paired myoblast cultures at 24 and 48 h after seeding. Despite resting $[Ca^{2+}]_i$ being depressed at 48 h (Fig. 3*A*), PEMFs remained capable of augmenting $[Ca^{2+}]_i$ to a comparable relative degree over baseline (Fig. 3*B*), although smaller in overall magnitude. Accordingly, PEMFs applied at 48 h produced less proliferation enhancement (Fig. 3*C*). Plating myoblasts at higher density quickens the onset of differentiation and, accordingly, prevented response to PEMFs as early as 24 h (Supplemental Figs. S3 and S5). Both cyclin D1 (Fig. 3*D*) and MyoD (Fig. 3*E*) levels were increased by PEMF exposure in low-density, but not high-density, cultures, indicating that both proliferation and differentiation would respond preferentially to early exposure (also see Supplemental Fig. S6). Our described electromagnetic efficacy window (Fig. 2*D–I*) was also lost at higher myoblast density (Supplemental Fig. S3*E, F*), indicating mitigation of magnetic sensitivity instead of shift in sensitivity. TTX did not uncover a response to PEMFs at 48 h (Fig. 3*F, G*) or at high cell densities (Fig. 3*G*), indicating that the expression of voltage-gated sodium channels (linked with differentiation) were not electrophysiologically masking an effect of the fields. Alternatively, loss of PEMF response may arise from the depletion of enabling trophic factors at longer culturing times or at higher cell densities. Refreshing culturing medium immediately before PEMF exposure at 48 h, or at high cell density, however, did not expose a hidden response to PEMFs (Supplemental Fig. S7). Consistent, with the up-regulation of MyoD with early PEMF exposure, early PEMF exposure also promoted differentiation. Exposure before 24 h postplating produced larger myotubes (Fig. 3*H*, blue) than exposure at 48 h (black). Moreover, continual PEMF exposure mitigated myotube formation (Fig. 3*I*; hatched) relative to singly exposed myoblasts (<24 h; blue) as well as controls (red). These results indicate that the calcium entry pathway implicated in this form of magnetoreception remains operational, albeit down-regulated, at 48 h.

We investigated the effects of pharmacological blockade of TRPC1 with 2-APB (22) at early (24 h) and later (48 h) time points to better ascertain specificity of magnetic fields. Though 2-APB (10 μM) was capable of preventing response to PEMFs at 24 h, it was ineffective at 48 h (Fig. 4*A*). SKF-96365 (50 μM Fig. 4*B*) (22) was also capable of preventing response to the fields at 24 h, strengthening the case for TRPC contribution. By contrast, inhibition of TRPM7 (10 mM $[Mg^{2+}]_e$) (24) was without effect (Fig. 4*C*). TRPV4 is the only other TRP

channel exhibiting an early expression pattern similar to TRPC1 (Supplemental Fig. S4*C*). Nonetheless, blocking TRPV4 channels with ruthenium red (10 μM; inset) (25), had no effect on PEMF response. Moreover, both TRPM7 (26) and TRPV4 (27) are insensitive to SKF-96365 and 2-APB at the concentrations used in this study, whereas TRPV3 is activated by 2-APB (28), corroborating specificity for TRPC channels. Finally, sensitivity to PEMFs paralleled the early expression pattern of TRPC1 (with reference to other TRPCs) (Supplemental Fig. S4) (6).

We selected a class of TRPC1 channel antagonists of minimal collateral cytotoxicity and high reversibility with which to emulate and better understand our magnetic responses. The aminoglycoside antibiotics have been demonstrated to antagonize TRPC1 in muscle (17). The aminoglycoside antibiotics were capable of preventing magnetically induced myogenic responses. Momentary application and then removal of aminoglycoside antibiotics, timed to coincide with PEMF exposure (10 min), was sufficient to block both PEMF-induced myoblast proliferation and differentiation (Fig. 4*D*–*M*), whereas identical application before PEMF exposure was not (Fig. 4*D*, inset). The antimyogenic effects of the aminoglycoside antibiotics are hence directly related to their capacity to interrupt PEMF-induced calcium entry (Fig. 4*M*) and recapitulating the effects of CsA (Fig. 4*N*, *O*).

Magnetic stimulation produced myogenic epigenetic responses that correlated with early TRPC1 expression pattern *in vitro* (6) (Fig. 3 and Supplemental Fig. S4). The protein levels of PCAF, a histone acetyltransferase and myogenin and MyoD transcriptional activator (29–31), were enhanced by PEMF exposure at 24 h (Fig. 5*A*) but not 48 h (Fig. 5*B*), as were the levels of PCAF's histone target, acetylated histone [^{3}H] at lysine residue 9 (H3K9ac) (Fig. 5*C*). MyoD expression also increased after early (24 h) exposure (Fig. 5*A*), reflecting its activation by PCAF acetylation (29–31) that, in combination with calcineurin/calcium-dependent activation of NFAT (32), promotes myogenic differentiation.

Contrasting with the effects of supplemental pulsing fields, magnetically isolating myoblasts from all ambient magnetic fields using a μ-metal housing (Supplemental Fig. S1*B*) instead reduced PCAF and H3K9ac protein levels (Fig. 5*D*). The aminoglycoside antibiotics were capable of recapitulating the reductions in PCAF and H3K9ac protein levels produced by magnetic shielding (Fig. 5*E*). Furthermore, both magnetic shielding (Fig. 5*F*) and conventional use of PS (Fig. 5*G*) reduced TRPC1 expression, indicating feedback regulation of TRPC1 (Fig. 3*C*). These results strengthen the case that magnetic fields target TRPC1 and support the conclusion that ambient magnetism is capable of modulating basal myogenesis by regulating TRPC1 function.

We investigated whether inhibiting calcineurin could defer oxidative determination following PEMF exposure. CsA reversed the characteristic PEMF-induced rise in PCAF at 24 h (Fig. 5*H*), whereas it had little effect at 48 h, consistent with its ability to block PEMF-induced differentiation (Fig. 4*N*, *O*). PEMF exposure also enhanced the nuclear translocation of NFATC1, whereas NFATC3 nuclear localization was reduced (Fig. 5*I* and Supplemental Fig. S8). Importantly, the nuclear translocation of NFATC1 has been shown to reflect a myogenic proclivity toward an oxidative phenotype (33), whereas the induction of oxidative muscle by PGC-1α does not appear to require the cooperation of NFATC3 (13). Inhibiting

calcineurin signaling thus impedes magnetically enhanced myogenesis at the levels of proliferation (Fig. 2*C*, inset), differentiation (Fig. 2*I*), and oxidative directive (Fig. 5*H*).

Immediate mitochondrial responses

Given the importance of mitochondria for oxidative muscle development (13), we examined the mitochondrial ramifications of our magnetic stimulation paradigm. Exposure to PEMFs stimulated the production of ROS (Fig. 6*A, B*) and ATP (Fig. 6*A*; inset), recapitulating our electromagnetic efficacy window governing myogenesis at the level of the mitochondria (Fig. 2 and Supplemental Fig. S3). On the one hand, PEMF-stimulated proliferation of myoblasts could be precluded by antioxidants (Fig. 6*C*), whereas ROS production could be inhibited by SKF 96365 or PS (Fig. 6*D*), linking TRPC1-mediated calcium entry to mitochondrial respiration with myogenic consequences. PEMF exposure increased mitochondrial OCR (Fig. 6*E*) that was sensitive to inhibition of TRPC1 (Fig. 6*F*). Paralleling myoblast proliferation (Fig. 3*D* and Supplemental Figs. S3 and S5) and differentiation (Fig. 3*E*), the PEMF-induced rise in OCR was lost at higher cell density (Fig. 6*G–J* and **Table 2**). Notably, myoblasts harvested at low density (low ρ; undifferentiated) and exposed to PEMFs while in suspension, followed by direct plating at high density a few hours prior to OCR measurement (before differentiation develops), did not preclude a response to PEMFs (Fig. 6*K, L*), whereas myoblasts harvested at high density (high ρ; differentiated) seeded and exposed in the same manner were instead magnetically insensitive (Table 2), corroborating that magnetosensitivity is developmentally regulated, likely associated with TRPC1 levels, rather than an effect of cell density *per se*. PEMF-treated myoblasts also exhibited an elevation in ECAR (Fig. 6*I, J, L*), indicating an increase in maximum cellular glycolytic capacity (34). The gray-shaded areas depict the additional spare respiratory capacity afforded by PEMF exposure, coinciding with elevated basal respiration and enhanced mitochondrial ATP production (Table 2) and preferentially sensitive to TRPC antagonism (Fig. 6*F*). Mitochondrial responses to PEMFs thus recapitulated the detected TRPC1 dependency of magnetic myogenic induction.

TRPC1 silencing abrogates PEMF-enhanced myogenesis and mitochondrial respiratory capacity

Gene silencing with either of 2 dsiRNAs (dsi1, dsi2) decreased TRPC1 expression by 74 and 56%, respectively (Fig. 7*A, B*), coinciding with a complete loss of proliferative response to PEMF exposure (Fig. 7*C*). By contrast, myoblasts transfected with a nontargeted scrambled (Scr) dsiRNA exhibited proliferative responses to PEMFs comparable to nontransfected myoblasts (control; Con), 25 and 39%, respectively (Supplemental Fig. S3). TRPC1-silencing decreased basal cyclin D1 levels by ~10% that, moreover, were unresponsive to PEMF exposure. By contrast, control myoblasts (Con, Scr) responded to PEMF exposure with a 15% increase in cyclin D1 levels (Fig. 7*A*; *cf.* Fig. 3*D*). Myoblasts in which TRPM7 had been silenced (Fig. 7*D*) exhibited typical PEMF-induced proliferative responses, 28% (ds1) *vs.* 34% (Scr) (Fig. 7*E*). CRISPR/Cas9-targeted deletion of TRPC1 exon 1 (Supplemental Fig. S9*D, E*) also produced a loss of PEMF sensitivity (Fig. 7*F*), associated with the reduced levels (Fig. 7*G*) of a truncated protein (~8 kDa; Supplemental Fig. S9*C*).

Removal of exon 1 of the TRPC1 genomic coding sequence thus appears to be sufficient to preclude sensitivity to PEMFs.

Two hallmark features of our reported magnetic responses are TRPC1 dependency and a discrete electromagnetic efficacy window (Fig. 1 and Supplemental Fig. S3). We sought to determine if these 2 key features are directly manifested at the level mitochondrial function. CRISPR/Cas9-mediated knockdown of TRPC1 abrogated the enhancement in mitochondrial respiratory capacity in response to magnetic stimulation. Notably, the absolute amplitude of the spare respiratory capacity and basal respiration (**Fig. 8*A–C***) were correlated with the level of TRPC1 knockdown previously noted (Fig. 7*G*). The c60 and c61 TRPC1-knockdown clones exhibited either no response or a modest reduction in OCR following PEMF exposure, respectively, that was similar to the inhibitory response observed in myoblasts plated at high density (30 K) (Table 2), further corroborating that loss of TRPC1 expression underlies the inhibitory effect of high cell density (Fig. 2 and Supplemental Fig. S4). Extracellular acidity increased in the TRPC1 knockdowns (Fig. 8*D–F*), indicating an increased reliance on anaerobic glycolysis outside the mitochondria (reduced mitochondrial respiration) when TRPC1 expression is knocked down. Our reported magnetic efficacy window (Fig. 2 and Supplemental Fig. S3) is also recapitulated at the level of the mitochondria (Fig. 8*G–L*; also see Fig. 6*A*) and, moreover, was sensitive to blockage by SKF-96365. These results confirm a mitochondrial-TRPC1 interplay activated by magnetic fields.

Adaptive mitochondrial responses

PGC-1α is a master regulator of mitochondriogenesis recruited by energy metabolism and calcium/calcineurin, typically in response to muscular activity (13, 35). Accordingly, PGC-1α transcript (PPARGC1A) levels increased post-PEMF exposure (Fig. 9*A*). PGC-1α expression is also subject to calcineurin (Figs. 2*C, I* and 4*N, O* and and5*H*)5*H*) regulation *via* its activation of NFATC1 (36, 37) (Fig. 5*I*) and myocyte-specific enhancer factor 2C (Mef2c) (13, 37–39), preferentially in oxidative muscle (13, 33). Mef2c (MEF2C) transcript expression was highest at 24 h post-PEMF exposure (Fig. 9*B*). Underscoring the role that mitochondrial activation has over oxidative muscle determination (35, 40), elevations in MyoD (MYOD1; Fig. 9*C*) and myogenin (MYOG; Fig. 9*D*) were most pronounced at 48 and 24 h following PEMF exposure, respectively, resulting in a ratio of myogenin to MyoD of >1 at 24 h (Fig. 9*E*), a transcriptional scenario predictive of subsequent oxidative muscular determination (*cf.* Fig. 5*I*) (40). Mitochondrial respiratory capacity and PGC-1α expression have also been linked to telomere maintenance (41). Correspondingly, telomerase reverse transcriptase (TERT) levels were increased following PEMF exposure (Fig. 9*F*), mirroring the positive association of telomere length with metabolic balance resulting from exercise (41, 42). TRPC1 expression was also augmented by brief PEMF exposure (Fig. 9*G*) (11), exhibiting the opposite trend (albeit at the protein level) observed with either magnetic shielding (Fig. 5*F*) or PS treatment (Fig. 5*G*). Knockout of PGC-1α in mice results in reduced muscular mitochondrial content and heightened apoptosis (43). In accordance with the increased expression of PGC-1α in response to PEMF exposure (Fig. 9*A*), mitochondriogenesis (mitochondrial DNA content) was enhanced (Fig.

9*H, I* and Supplemental Fig. S10*A*) and basal cell death reduced (Fig. 9*J*) post-PEMF exposure. Caspases-3 and -9 and Bcl-xL have been shown to synergize to promote myogenesis (44, 45), whereby Caspase-3 stops the expansion of satellite cells (45). Accordingly, cleaved Caspases 3 and 9 (Fig. 9*K*) and BcL-xL (Fig. 9*L*) were all reduced 48 h after PEMF exposure, aligning with the detected antiapoptotic (Fig. 9*J*), proproliferative and promyogenic properties of PEMF stimulation demonstrated throughout this report (Supplemental Fig. S10*B, C*). We therefore observe both immediate (Figs. 6 and and8)8) and adaptive (Fig. 9) mitochondrial responses following brief magnetic field exposure with ultimate implications to cell survival.

Magnetic specificity

Diverse tests were conducted to ascertain magnetic specificity of our demonstrated myogenic responses. During exposure, myoblasts were placed within a μ-metal housing capable of shielding cells from all incoming magnetic stimulation while still subjecting them to all other exogenous stimuli inherent to the PEMF-delivery system (Supplemental Fig. S1*C*). Shielding myoblasts in such a manner precluded a response to our pulsing fields (Fig. 10*A*). To exclude the possibility of stimulatory mechanical artifacts, we vibrated myoblast cultures at the same frequency and magnitude as they might experience during normal exposure. This level of vibration alone was insufficient to enhance proliferation (Fig. 10*B*). Myoblasts in suspension also responded to PEMFs at the levels of proliferation (Fig. 10*C*) and mitochondrial respiration (Fig. 6*K*), further arguing against substrate-mediated contractile stresses being a predominant force underlying our observed magnetic responses. Lastly, growing myoblasts in magnetic isolation (Supplemental Fig. S1*B*) down-regulated the same TRPC1/NFAT/PCAF myogenic cascade that was up-regulated by supplementary PEMFs (Fig. 5 and Supplemental Fig. S1*A*), corroborating that ambient magnetic fields (k_BT) are relevant and sufficient to promote myogenesis, without altering the mechanical environment of myoblasts. These control scenarios indicate that the magnetic stimulation paradigm employed in this study does not inadvertently provide mechanical stimulation, directly or indirectly. The sum of our data thus indicates that skeletal muscle is explicitly developmentally responsive to magnetic fields *via* a mitochondria-targeted signaling complex containing, among other yet-to-be-determined molecular entities, TRPC1.

DISCUSSION

TRPC1, an integrator of biological responses

Sensitivity to magnetic fields specifically follows TRPC1 expression developmentally (Figs. 3–5 and and10,10, and Supplemental Fig. S4) (6), genetically (Figs. 7 and and8),8), and pharmacologically (Figs. 2, ,44–6, ,8,8, and and10).10). TRPC1 has previously been ascribed roles in mechanotransduction and store-operated calcium entry (SOCE) (4). TRPC1-mediated calcium entry stimulates myoblast proliferation, whether activated *via* its mechanosensitive or SOCE (6) gating modes. Accordingly, TRPC1 expression was correlated with mechanosensitivity, SOCE, and proliferative capacity within the same populations of myoblasts (6), underscoring its role as an integrator of diverse stimuli. Here

we extend the list of functions attributed to TRPC1 by revealing for it roles in magnetoreception and redox homeostasis.

Both continual PEMF exposure (Fig. 3*I*) and sustained mechanical stimulation (46) are capable of deferring MyoD, coincident with the reexpression of TRPC1 (Fig. 3*C*, inset) (47). Brief exposure to PEMFs was also capable of reversing the slowing of proliferation (Fig. 10*D*) produced by simulated microgravity (μ*g*) and correlated with a drop in TRPC1-mediated calcium entry in myoblasts (6, 12). Magnetoreception and mechanosensitivity thus employ a common transduction pathway impinging on TRPC1 and are capable of acting independently (see Magnetic Specificity) as well as synergistically.

Comparison with state of the art

The pulsing magnetic fields we employed in this study are within the amplitude range typically used by others (low mT) (14), but uniquely, revealing a discrete response window defined by timing, duration of exposure, as well as amplitude (Figs. 2 and and8,8, and Supplemental Fig. S3). First, we obtain the best results with much briefer exposure times (10 min, applied once) than previously reported (>h/wk) (16). Our magnetic stimulation protocol also differs from convention in terms of timing of exposure. Critically, we administered PEMFs much earlier (<24 h postplating) and at a much lower density than most investigators, who typically prefer to permit cells to reach higher confluence before exposure. Differences in developmental efficacy with respect to previously published studies may hence arise from: *1*) the stimulation of a cell type/tissue outside of its inherent efficacy window (Figs. 2 and and8,8, and Supplemental Fig. S3); *2*) field application during an inappropriate developmental stage *in vitro* (Figs. 3–5, and Supplemental Fig. S4); *3*) repetitive/excessive stimulation (Fig. 3*I*); *4*) cell overgrowth or senescence at the time of stimulation (Figs. 3 and and6,6, and Supplemental Figs. S3 and S5); *5*) the use of aminoglycoside antibiotics (Figs. 4–6 and and10)10) (17); *6*) contributing electromagnetic stimulation arising from the environment (Fig. 5) (48); *7*) cellular oxidative stress at the time of measurement (Fig. 6); or *8*) any combination of the above factors.

Weak static magnetic fields gave qualitatively similar results (49) to those reported here. Despite obvious differences in amplitude (<200 μT), mode (constant), and treatment duration (2 wk), this *in vitro* study *1*) extrapolated our findings to primary muscle cells, *2*) corroborated that magnetic fields induce increments in myoplasmic calcium (Fig. 2), *3*) confirmed that magnetic fields promote myogenic differentiation (Figs. 2–5), *4*) revealed a magnetic efficacy window whereby stronger static fields (>400 μT) were less myogenic (Figs. 2 and and8,8, and Supplemental Fig. S3), *5*) demonstrated that differentiated muscle cells were less responsive to magnetic fields (Figs. 3–5), and *6*) established that magnetic fields on the order of those present environmentally are sufficient to support basal myogenesis (Fig. 5). However, the pulsing fields described here required only brief (10 min), single exposure to accentuate *in vitro* myogenesis.

A TRPC1 mitochondrial axis underlies magnetoreception

Magnetoreception is an accepted biological phenomenon (50) with demonstrated relevance to mitochondrial function and myogenesis (14, 15, 51). Shielding stem cells from the earth's magnetic field (45–60 μT) diminished pluripotency (52) and mitochondrial respiratory capacity (53), paralleling our findings that μ-metal isolation of myoblasts depressed myogenesis (Fig. 5), whereas supplemental magnetic fields stimulated myogenesis (Figs. 2–5 and and9),9), mitochondrial respiratory capacity, and ROS production (Figs. 6 and and8,8, and Table 2). These results suggest that we are harnessing a *bona fide* magnetic response encompassing mitochondrial modulation of myogenesis.

Mitochondria are potent regulators of myogenesis (54, 55) that work in cohort with the calcineurin/NFAT catalytic cascades for myogenic enhancement (54) and adaptive metabolic responses (55, 56). Earlier findings have separately demonstrated that both ROS (57) and TRPC1 (6, 12, 23) promote myogenesis. Other studies have directly linked ROS production with TRPC1-mediated calcium entry (58, 59). In this report, we extend the existing state of understanding by showing that the magnetic modulation of mitochondrial respiration in skeletal muscle requires the participation of TRPC1-mediated calcium entry for myogenic outcome (Figs. 6 and and8,8, and Table 2).

The effects that weak magnetic fields have been shown to exert over mitochondrial function (53) exhibit mechanistic commonalities with known quantum biological phenomena (50, 51). The radical-pair mechanism is an established precept in quantum biological processes that commonly centers around flavin radical-pair production (60), wherein electron singlet to triplet spin transitions are favored by weak magnetic fields of the correct temporal characteristics, facilitating the production of bioactive radicals. Notably, radical-pair interactions are thermally isolated such that the magnetically tuned radical-pair mechanism is operational under ambient conditions, free of having to possess sufficient energy of interaction to surpass ambient k_BT (60). This feature aligns with our data showing that pharmacological antagonism of TRPC channels under resting conditions (Figs. 2*B* and 5*E, G*) or magnetic isolation from ambient magnetism (Fig. 5*D, F*) reverts basal myogenesis, corroborating that magnetism is capable of sustaining myogenesis at k_BT. Lastly, it has been recently shown that ROS production arising from the transfer of electrons from reduced flavoenyzmes to molecular oxygen (O_2) is magnetically modulated and manifests itself as an enhancement of mitochondrial OCRs (Figs. 6 and and8,8, and Table 2) (61). Quantum biological processes are hence likely being played out at the level of mitochondrial energy production (51).

We show that both ambient and applied pulsing magnetic fields in an extremely low frequency range (Hz-low kHz) employ identical transduction mechanisms (TRPC1) and downstream genetic and epigenetic developmental cascades to modulate myogenesis. The supplemental magnetic fields employed in this study are only 20–30 times greater in amplitude (1–1.5 mT) than the earth's standing field (~50 μT) (50, 52, 54). Of relevance, it has been recently shown that applied low-frequency magnetic fields in the range of 1 mT are capable of radical-pair amplification generated by flavin-tryptophan moieties, whereas amplitudes exceeding the hyperfine nuclear interactions limit (~3 mT) are inefficient at doing so (62), perhaps giving insight as to the origin of the myogenic efficacy amplitude ceiling of the pulsing magnetic fields described in this report (Supplemental Fig. S3).

Magnetic mitohormesis

ROS and Ca^{2+} are myogenically stimulatory and yet are cytotoxic at critical doses (58, 59). Hormesis refers to a process whereby a stressor at low doses induces an adaptive response that later confers upon an organism greater survival to the same stress (51, 63); exercise is hormetic. A TRPC1-mitochondrial interplay may establish a mitohormetic (mitochondrial hormesis) level of ROS (15, 51, 63) that underlies the temporal dosage characteristics of our magnetic efficacy window (Supplemental Fig. S3), whereby protracted or repeated exposures produce excessive amounts of ROS that are counterproductive to myogenic progression. Obeying mitohormesis, healthy skeletal muscle cells will be capable of adapting to brief and low-amplitude magnetic exposure with increased resistance to subsequent oxidative stress and will be manifested as enhanced survival (Fig. 9), whereas unadapted muscle cells, concomitantly experiencing oxidative stress and subjected to the same exposure, will likely respond adversely to the cumulative ROS production (50, 51, 63). A key participant in this adaptive response to imminent oxidative stress would be PGC-1α (Fig. 9*A*), which has been shown to be both up-regulated by ROS (64) and attenuates ROS-mediated removal of mitochondria during myogenesis (65). TRPC1-mediated calcium influx would also participate in this ROS-myogenesis regulatory axis by responding to ROS creation with enhanced calcium entry that, moreover, is subject to blockade by the aminoglycoside antibiotics (59). Our finding that ambient magnetism sustains basal myogenesis (Fig. 5) is consistent with the existence of a mitohormetic myogenic mechanism (51, 63), monitoring and adapting to the environment, as well as reflecting its quantum biological origin (50, 60, 62). The electromagnetic efficacy window described in this study (Supplemental Fig. S3) thus fulfils obligate criteria of a quantum biologically assisted mitohormetic process.

In line with the hormetic interpretation, a recent report has shown that prolonged (48 h) exposure to 1.8 mT pulsing magnetic fields halted cell proliferation and was associated with ROS production *via* cryptochrome (*cry2*) (66), a mammalian magnetoreceptor known to undergo flavin adenine dinucleotide–dependent radical-pair formation. This finding aligns with our demonstrated anti-proliferative capacity of excessive exposure to pulsing fields (Figs. 2 and and3,3, and Supplemental Fig. S3) and may relate to existing evidence of functional interaction between cytosolic calcium levels and cryptochrome function (67). Electromagnetic photoactivation of a cryptochrome in *Drosophila melanogaster* has also been shown to be functionally coupled to the redox-sensor of a conserved potassium channel subunit required for neurologic magnetic field detection (68), hinting at the existence of a conserved mood of interaction between radical-pair–based forms of magnetoreception and ionic fluxes, essentially bridging the transduction event to cellular response. The possibility thus exists of multiple flavin pathways contributing to magnetoreception. Future studies should investigate the mechanisms of interactions between magnetically modulated flavin radical mechanisms (crytochrome or mitochondrial) and TRP channel–mediated calcium entry as well as how such quantum biological processes may contribute to establishing a ROS-tuned hormetic modulatory cascade.

TRP channel developmental analysis

TRPC1 and TRPM7 are the most abundantly and ubiquitously expressed of all TRP channels, underscoring their physiologic and developmental importance (69). Our developmental (Figs. 3 and and5),5), pharmacological (Fig. 4), and genetic (Figs. 7 and and8)8) dissections of the contribution of these 2 TRP channels in magnetoreception indicate a predominant role for TRPC1. Magnetic sensitivity also coincides with TRPC1 *in vitro* expression at the functional (5), transcriptional (6), and protein levels (Supplemental Fig. S4). With the exception of TRPC6, channel protein expression was modulated between 24 and 48 h. Notably, TRPV4 expression paralleled the drop in TRPC1 expression observed at 48 h. Nonetheless, despite TRPV4 following a similar expression pattern as TRPC1 (Supplemental Fig. S4), PEMF responses were inhibited by 2-APB (Figs. 2 and and4)4) and unaltered by ruthenium red (Supplemental Fig. S4*C*; inset), diametrically opposed with the described 2-APB insensitivity (27) and ruthenium red sensitivity (25, 28) of TRPV4, suggesting that TRPV4 is not involved in magnetic sensing. In mesenchymal stromal cells undergoing PEMF-induced chondrogenesis, however, TRPV4 expression similarly followed that of TRPC1 and again exhibited antagonism to 2-APB (20), recapitulating the same TRP-expression/function pattern as skeletal muscle. The reoccurrence of this trend suggests an interplay between TRPV4 with TRPC1 (70) while further extending the evidence for an involvement of TRPC1 in magnetoreception to another mechanosensitive tissues. The sum of our results thus lean toward a principal role for TRPC1 in magnetotransduction, although the potential contributions from other TRP channels, either directly or indirectly, cannot be excluded at this time.

Conventional TRP channel pharmacology is notoriously promiscuous, widely disparate in effects among the different channel subtypes, and associated with a multitude of collateral effects (22, 28). We chose the aminoglycoside antibiotics to pharmacologically emulate the effects of magnetic shielding principally for their high reversibility, simple mechanism of blockage, and relatively low cytotoxicity, which eased interpretation of the results. The aminoglycoside antibiotics have been shown to sterically impede calcium permeation (open channel block) through small-conductance mechanically gated cation channels in skeletal muscle (71) as well as antagonize TRPC1 in muscle (17, 59) where they are thought to represent the same or related entities (5–9). Despite the inference that the detected “stretch-activated” and TRP channels in skeletal muscle are synonymous, the capacity of the aminoglycoside antibiotics to block magnetic responses is supported by our results and is of high biological relevance. The aminoglycoside antibiotics were found capable of inhibiting the effects of magnetic fields with minimal exposure, applied only during brief magnetic exposure and then rapidly replaced with age-matched medium harvested from sister cultures, indicating a direct mechanism of interaction rather than a biosynthetic form of interruption of a more protracted time course. Such a response is consistent with a rapid and direct channel-blocking scheme, as previously shown (71) and demonstrates a form of magnetic specificity that correlates on several levels with TRPC1 expression and pharmacology. Our findings demonstrate direct competition between the aminoglycoside antibiotics and magnetism for TRPC1 (Figs. 4–6 and and10).10). PS also only significantly down-regulated the protein expressions of TRPC1 (24 and 48 h), TRPC6 (24 and 48 h), and TRPV4 (48 h) (Supplemental Fig. S4).

In summary, we provide compelling evidence that magnetism is an authentic myogenic stimulus. *In vitro* myogenesis was enhanced by unprecedentedly brief (10 min), single exposures to low-amplitude pulsing magnetic fields. Magnetic fields, both supplemental and ambient, mediate their effects by activating TRPC1-mediated calcium entry and mitochondrial respiration downstream of calcineurin-dependent transcriptional regulation and PCAF-epigenetic cascades previously implicated in myogenesis, whereas shielding myoblasts from ambient magnetic fields revert these responses. The myogenic effects of magnetic fields could also be blocked by aminoglycoside antibiotics because of their capacity to attenuate TRP channel function, warning against their use during such studies.

ACKNOWLEDGMENTS

The authors acknowledge Dr. T. Benavides Damm [Swiss Space Center, Swiss Federal Institute of Technology (ETH Zurich)] for assisting with the simulated microgravity experiment shown in Fig. 10*D*, and Dr. Krzysztof Krawczyk (ETH Zurich) for assistance in conducting the fusion index histogram in Fig. 3*H*. The authors also acknowledge Zac Goh (iHealthtech, National University of Singapore) for the design of graphical abstract shown in Fig. 1. This study was financially supported by the European Space Agency Grant ESA-CORA-GBF (4000113883), the Fondation Suisse de Recherche sur les Maladies Musculaires, and the Lee Foundation, Singapore. J.F., C.B., C.N.L., and A.F.-O. are inventors on patent WO 2016/178631 A1, System and Method for Applying Pulsed Electromagnetic Fields, and J.F., C.N.L. and A.F.-O. are contributors to QuantumTx Pte. Ltd., which elaborates on the use of similar magnetic fields on human health (targeting muscle). The other authors declare no conflicts of interest.

Glossary

B2M	β-2 microglobulin
$[Ca^{2+}]_i$	intracellular $[Ca^{2+}]$ concentration
2-APB	2-aminoethoxydiphenylborate
CRISPR	clustered regularly interspaced short palindromic repeats
CsA	cyclosporin A

dsiRNA	dicer-substrate interfering RNA
ECAR	extracellular acidification rate
FACS	fluorescence-activated cell sorting
FBS	fetal bovine serum
GAPDH	glyceraldehyde 3-phosphate dehydrogenase
GM	growth medium
$k_{\mathrm{B}}T$	thermal energy
Mef2c	myocyte-specific enhancer factor 2C
MyoD	myogenic differentiation
NFAT	nuclear factor of activated T cells
OCR	oxygen consumption rate
PS	penicillin/streptomycin

PCAF	P300/CBP-associated factor
PEMF	pulsed electromagnetic field
PGC-1α	peroxisome proliferator–activated receptor γ coactivator 1α
ROS	reactive oxygen species
RPM	random positioning machine
Scr	scrambled
sgRNA	single-guide RNA
SOCE	store-operated calcium entry
TRP	transient receptor potential
TRPM7	transient receptor potential melastatin 7
TTX	tetrodotoxin

Footnotes

This article includes supplemental data. Please visit *http://www.fasebj.org* to obtain this information.

AUTHOR CONTRIBUTIONS

A. Franco-Obregón conceptualized and designed the study, developed protocols, collected, assembled, analyzed, and interpreted data as well as composed the manuscript and obtained financial support for the study; J. Fröhlich helped conceptualize and design the study, obtained funding, and provided engineering and technical expertise; J. L. Y. Yap and Y. K. Tai developed and optimized protocols, collected, assembled, analyzed data, and assisted in the writing of the manuscript; C. Beyer assisted with engineering, technical and experimental design, and data collection; C. H. H. Fong, J. N. Yin, Z. L. Foo, S. Ramanan, S. J. Toh, M. Casarosa, N. Bharathy, and M. P. Kala collected, assembled, and analyzed the data; M. Egli, R. Taneja, and C. N. Lee provided infrastructural and financial support; and all authors approved the final version of the manuscript.

Supplementary Material

This article includes supplemental data. Please visit *http://www.fasebj.org* to obtain this information.

REFERENCES

1. Cheng C. F., Ku H. C., Lin H. (2018) PGC-1α as a pivotal factor in lipid and metabolic regulation. *Int. J. Mol. Sci.* 19, E3447 [PMCID: PMC6274980] [PubMed: 30400212]

2. Goodpaster B. H., Sparks L. M. (2017) Metabolic flexibility in health and disease. *Cell Metab.* 25, 1027–1036 [PMCID: PMC5513193] [PubMed: 28467922]

3. Fraysse B., Desaphy J. F., Pierno S., De Luca A., Liantonio A., Mitolo C. I., Camerino D. C. (2003) Decrease in resting calcium and calcium entry associated with slow-to-fast transition in unloaded rat soleus muscle. *FASEB J.* 17, 1916–1918 [PubMed: 12923063]

4. Eijkelkamp N., Quick K., Wood J. N. (2013) Transient receptor potential channels and mechanosensation. *Annu. Rev. Neurosci.* 36, 519–546 [PubMed: 23750514]

5. Franco A., Jr., Lansman J. B. (1990) Stretch-sensitive channels in developing muscle cells from a mouse cell line. *J. Physiol.* 427, 361–380 [PMCID: PMC1189935] [PubMed: 2170636]

6. Crocetti S., Beyer C., Unternährer S., Benavides Damm T., Schade-Kampmann G., Hebeisen M., Di Berardino M., Fröhlich J., Franco-Obregón A. (2014) Impedance flow cytometry gauges proliferative capacity by detecting TRPC1 expression. *Cytometry A* 85, 525–536 [PubMed: 24639248]

7. Zanou N., Schakman O., Louis P., Ruegg U. T., Dietrich A., Birnbaumer L., Gailly P. (2012) Trpc1 ion channel modulates phosphatidylinositol 3-kinase/Akt pathway during myoblast differentiation and muscle regeneration. *J. Biol. Chem.* 287, 14524–14534 [PMCID: PMC3340236] [PubMed: 22399301]

8. Xia L., Cheung K. K., Yeung S. S., Yeung E. W. (2016) The involvement of transient receptor potential canonical type 1 in skeletal muscle regrowth after unloading-induced atrophy. *J. Physiol.* 594, 3111–3126 [PMCID: PMC4887677] [PubMed: 26752511]

9. Zanou N., Shapovalov G., Louis M., Tajeddine N., Gallo C., Van Schoor M., Anguish I., Cao M. L., Schakman O., Dietrich A., Lebacq J., Ruegg U., Roulet E., Birnbaumer L., Gailly P. (2010) Role of TRPC1 channel in skeletal muscle function. *Am. J. Physiol. Cell Physiol.* 298, C149–C162 [PMCID: PMC2806157] [PubMed: 19846750]

10. Frey N., Frank D., Lippl S., Kuhn C., Kögler H., Barrientos T., Rohr C., Will R., Müller O. J., Weiler H., Bassel-Duby R., Katus H. A., Olson E. N. (2008) Calsarcin-2 deficiency increases exercise capacity in mice through calcineurin/NFAT activation. *J. Clin. Invest.* 118, 3598–3608 [PMCID: PMC2564612] [PubMed: 18846255]

11. Morales S., Diez A., Puyet A., Camello P. J., Camello-Almaraz C., Bautista J. M., Pozo M. J. (2007) Calcium controls smooth muscle TRPC gene transcription via the CaMK/calcineurin-dependent pathways. *Am. J. Physiol. Cell Physiol.* 292, C553–C563 [PubMed: 16956967]

12. Benavides Damm T., Franco-Obregón A., Egli M. (2013) Gravitational force modulates G2/M phase exit in mechanically unloaded myoblasts. *Cell Cycle* 12, 3001–3012 [PMCID: PMC3875675] [PubMed: 23974110]

13. Lin J., Wu H., Tarr P. T., Zhang C. Y., Wu Z., Boss O., Michael L. F., Puigserver P., Isotani E., Olson E. N., Lowell B. B., Bassel-Duby R., Spiegelman B. M. (2002) Transcriptional co-activator PGC-1 alpha drives the formation of slow-twitch muscle fibres. *Nature* 418, 797–801 [PubMed: 12181572]

14. Wade B. (2013) A review of pulsed electromagnetic field (PEMF) mechanisms at a cellular level: a rationale for clinical use. *Am. J. Health Res.* 1, 51–55

15. Morabito C., Rovetta F., Bizzarri M., Mazzoleni G., Fanò G., Mariggiò M. A. (2010) Modulation of redox status and calcium handling by extremely low frequency electromagnetic fields in C2C12 muscle cells: a real-time, single-cell approach. *Free Radic. Biol. Med.* 48, 579–589 [PubMed: 20005945]

16. Xu H., Zhang J., Lei Y., Han Z., Rong D., Yu Q., Zhao M., Tian J. (2016) Low frequency pulsed electromagnetic field promotes C2C12 myoblasts proliferation via activation of MAPK/ERK pathway. *Biochem. Biophys. Res. Commun.* 479, 97–102 [PubMed: 27629357]

17. Matsumura C. Y., Taniguti A. P., Pertille A., Santo Neto H., Marques M. J. (2011) Stretch-activated calcium channel protein TRPC1 is correlated with the different degrees of the dystrophic phenotype in mdx mice. *Am. J. Physiol. Cell Physiol.* 301, C1344–C1350 [PubMed: 21900691]

18. Shalem O., Sanjana N. E., Hartenian E., Shi X., Scott D. A., Mikkelson T., Heckl D., Ebert B. L., Root D. E., Doench J. G., Zhang F. (2014) Genome-scale CRISPR-Cas9

knockout screening in human cells. *Science* 343, 84–87 [PMCID: PMC4089965] [PubMed: 24336571]

19. Ong E. C., Nesin V., Long C. L., Bai C. X., Guz J. L., Ivanov I. P., Abramowitz J., Birnbaumer L., Humphrey M. B., Tsiokas L. (2013) A TRPC1 protein-dependent pathway regulates osteoclast formation and function. *J. Biol. Chem.* 288, 22219–22232 [PMCID: PMC3829314] [PubMed: 23770672]

20. Parate D., Franco-Obregón A., Fröhlich J., Beyer C., Abbas A. A., Kamarul T., Hui J. H. P., Yang Z. (2017) Enhancement of mesenchymal stem cell chondrogenesis with short-term low intensity pulsed electromagnetic fields. *Sci. Rep.* 7, 9421 [PMCID: PMC5572790] [PubMed: 28842627]

21. Crocetti S., Beyer C., Schade G., Egli M., Fröhlich J., Franco-Obregón A. (2013) Low intensity and frequency pulsed electromagnetic fields selectively impair breast cancer cell viability. *PLoS One* 8, e72944 [PMCID: PMC3770670] [PubMed: 24039828]

22. Szallasi A. (2015) Are brain TRPs viable targets for curing neurodegenerative disorders and improving mental health? In *TRP Channels as Therapeutic Targets: From Basic Science to Clinical Use.* (Nilius B., Szallasi A.), pp. 419–456, Academic Press, London

23. Targos B., Barańska J., Pomorski P. (2005) Store-operated calcium entry in physiology and pathology of mammalian cells. *Acta Biochim. Pol.* 52, 397–409 [PubMed: 15933763]

24. Wei C., Wang X., Chen M., Ouyang K., Song L. S., Cheng H. (2009) Calcium flickers steer cell migration. *Nature* 457, 901–905 [PMCID: PMC3505761] [PubMed: 19118385]

25. Vincent F., Duncton M. A. (2011) TRPV4 agonists and antagonists. *Curr. Top. Med. Chem.* 11, 2216–2226 [PubMed: 21671873]

26. Kuras Z., Yun Y. H., Chimote A. A., Neumeier L., Conforti L. (2012) KCa3.1 and TRPM7 channels at the uropod regulate migration of activated human T cells. *PLoS One* 7, e43859 [PMCID: PMC3428288] [PubMed: 22952790]

27. Ho T. C., Horn N. A., Huynh T., Kelava L., Lansman J. B. (2012) Evidence TRPV4 contributes to mechanosensitive ion channels in mouse skeletal muscle fibers. *Channels (Austin)* 6, 246–254 [PMCID: PMC3508903] [PubMed: 22785252]

28. Hu H., Grandl J., Bandell M., Petrus M., Patapoutian A. (2009) Two amino acid residues determine 2-APB sensitivity of the ion channels TRPV3 and TRPV4. *Proc. Natl. Acad. Sci. USA* 106, 1626–1631 [PMCID: PMC2635798] [PubMed: 19164517]

29. Fauquier L., Azzag K., Parra M. A. M., Quillien A., Boulet M., Diouf S., Carnac G., Waltzer L., Gronemeyer H., Vandel L. (2018) CBP and P300 regulate distinct gene networks required for human primary myoblast differentiation and muscle integrity. *Sci. Rep.* 8, 12629 [PMCID: PMC6105712] [PubMed: 30135524]

30. Dilworth F. J., Seaver K. J., Fishburn A. L., Htet S. L., Tapscott S. J. (2004) *In vitro* transcription system delineates the distinct roles of the coactivators pCAF and p300

during MyoD/E47-dependent transactivation. *Proc. Natl. Acad. Sci. USA* 101, 11593–11598 [PMCID: PMC511026] [PubMed: 15289617]

31. Gao X., Pan W. S., Dai H., Zhang Y., Wu N. H., Shen Y. F. (2010) CARM1 activates myogenin gene via PCAF in the early differentiation of TPA-induced rhabdomyosarcoma-derived cells. *J. Cell. Biochem.* 110, 162–170 [PubMed: 20213728]

32. Armand A. S., Bourajjaj M., Martínez-Martínez S., el Azzouzi H., da Costa Martins P. A., Hatzis P., Seidler T., Redondo J. M., De Windt L. J. (2008) Cooperative synergy between NFAT and MyoD regulates myogenin expression and myogenesis. *J. Biol. Chem.* 283, 29004–29010 [PMCID: PMC2662004] [PubMed: 18676376]

33. Calabria E., Ciciliot S., Moretti I., Garcia M., Picard A., Dyar K. A., Pallafacchina G., Tothova J., Schiaffino S., Murgia M. (2009) NFAT isoforms control activity-dependent muscle fiber type specification. *Proc. Natl. Acad. Sci. USA* 106, 13335–13340 [PMCID: PMC2726382] [PubMed: 19633193]

34. Nicholls D. G., Darley-Usmar V. M., Wu M., Jensen P. B., Rogers G. W., Ferrick D. A. (2010) Bioenergetic profile experiment using C2C12 myoblast cells. *J. Vis. Exp.* 6, 2511 [PMCID: PMC3159644] [PubMed: 21189469]

35. Trewin A. J., Berry B. J., Wojtovich A. P. (2018) Exercise and mitochondrial dynamics: keeping in shape with ROS and AMPK. *Antioxidants* 7, E7 [PMCID: PMC5789317] [PubMed: 29316654]

36. Roberts-Wilson T. K., Reddy R. N., Bailey J. L., Zheng B., Ordas R., Gooch J. L., Price S. R. (2010) Calcineurin signaling and PGC-1alpha expression are suppressed during muscle atrophy due to diabetes. *Biochim. Biophys. Acta* 1803, 960–967 [PMCID: PMC2885580] [PubMed: 20359506]

37. Perroud J., Bernheim L., Frieden M., Koenig S. (2017) Distinct roles of NFATc1 and NFATc4 in human primary myoblast differentiation and in the maintenance of reserve cells. *J. Cell Sci.* 130, 3083–3093 [PubMed: 28760926]

38. Hudson M. B., Price S. R. (2013) Calcineurin: a poorly understood regulator of muscle mass. *Int. J. Biochem. Cell Biol.* 45, 2173–2178 [PMCID: PMC3947871] [PubMed: 23838168]

39. Kang C., Li Ji L. (2012) Role of PGC-1α signaling in skeletal muscle health and disease. *Ann. N. Y. Acad. Sci.* 1271, 110–117 [PMCID: PMC3499658] [PubMed: 23050972]

40. Hughes S. M., Chi M. M., Lowry O. H., Gundersen K. (1999) Myogenin induces a shift of enzyme activity from glycolytic to oxidative metabolism in muscles of transgenic mice. *J. Cell Biol.* 145, 633–642 [PMCID: PMC2185087] [PubMed: 10225962]

41. Sahin E., Colla S., Liesa M., Moslehi J., Müller F. L., Guo M., Cooper M., Kotton D., Fabian A. J., Walkey C., Maser R. S., Tonon G., Foerster F., Xiong R., Wang Y. A., Shukla S. A., Jaskelioff M., Martin E. S., Heffernan T. P., Protopopov A., Ivanova E., Mahoney J. E., Kost-Alimova M., Perry S. R., Bronson R., Liao R., Mulligan R., Shirihai O. S., Chin L.,

DePinho R. A. (2011) Telomere dysfunction induces metabolic and mitochondrial compromise. *Nature* 470, 359–365; erratum: 475, 254 [PMCID: PMC3741661] [PubMed: 21307849]

42. Arsenis N. C., You T., Ogawa E. F., Tinsley G. M., Zuo L. (2017) Physical activity and telomere length: impact of aging and potential mechanisms of action. *Oncotarget* 8, 45008–45019 [PMCID: PMC5546536] [PubMed: 28410238]

43. Adhihetty P. J., Uguccioni G., Leick L., Hidalgo J., Pilegaard H., Hood D. A. (2009) The role of PGC-1alpha on mitochondrial function and apoptotic susceptibility in muscle. *Am. J. Physiol. Cell Physiol.* 297, C217–C225 [PubMed: 19439529]

44. Murray T. V., McMahon J. M., Howley B. A., Stanley A., Ritter T., Mohr A., Zwacka R., Fearnhead H. O. (2008) A non-apoptotic role for caspase-9 in muscle differentiation. *J. Cell Sci.* 121, 3786–3793 [PubMed: 18957517]

45. Dick S. A., Chang N. C., Dumont N. A., Bell R. A., Putinski C., Kawabe Y., Litchfield D. W., Rudnicki M. A., Megeney L. A. (2015) Caspase 3 cleavage of Pax7 inhibits self-renewal of satellite cells. *Proc. Natl. Acad. Sci. USA* 112, E5246–E5252 [PMCID: PMC4586827] [PubMed: 26372956]

46. Kook S. H., Lee H. J., Chung W. T., Hwang I. H., Lee S. A., Kim B. S., Lee J. C. (2008) Cyclic mechanical stretch stimulates the proliferation of C2C12 myoblasts and inhibits their differentiation via prolonged activation of p38 MAPK. *Mol. Cells* 25, 479–486 [PubMed: 18443411]

47. Chen M. S., Xiao J. H., Wang Y., Xu B. M., Gao L., Wang J. L. (2013) Upregulation of TRPC1 contributes to contractile function in isoproterenol-induced hypertrophic myocardium of rat. *Cell. Physiol. Biochem.* 32, 951–959 [PubMed: 24107839]

48. Portelli L. A., Schomay T. E., Barnes F. S. (2013) Inhomogeneous background magnetic field in biological incubators is a potential confounder for experimental variability and reproducibility. *Bioelectromagnetics* 34, 337–348 [PubMed: 23457052]

49. Surma S. V., Belostotskaya G. B., Shchegolev B. F., Stefanov V. E. (2014) Effect of weak static magnetic fields on the development of cultured skeletal muscle cells. *Bioelectromagnetics* 35, 537–546 [PubMed: 25266690]

50. Lambert N., Chen Y. N., Cheng Y. C., Li C. M., Chen G. Y., Nori F. (2013) Quantum biology. *Nat. Phys.* 9, 10–18

51. Nunn A. V., Guy G. W., Bell J. D. (2016) The quantum mitochondrion and optimal health. *Biochem. Soc. Trans.* 44, 1101–1110 [PMCID: PMC5264502] [PubMed: 27528758]

52. Baek S., Quan X., Kim S., Lengner C., Park J. K., Kim J. (2014) Electromagnetic fields mediate efficient cell reprogramming into a pluripotent state. *ACS Nano* 8, 10125–10138 [PubMed: 25248035]

53. Martino C. F., Castello P. R. (2011) Modulation of hydrogen peroxide production in cellular systems by low level magnetic fields. *PLoS One* 6, e22753 [PMCID: PMC3162571] [PubMed: 21887222]

54. Wagatsuma A., Sakuma K. (2013) Mitochondria as a potential regulator of myogenesis. *ScientificWorldJournal* 2013, 593267 [PMCID: PMC3574753] [PubMed: 23431256]

55. Sin J., Andres A. M., Taylor D. J., Weston T., Hiraumi Y., Stotland A., Kim B. J., Huang C., Doran K. S., Gottlieb R. A. (2016) Mitophagy is required for mitochondrial biogenesis and myogenic differentiation of C2C12 myoblasts. *Autophagy* 12, 369–380 [PMCID: PMC4836019] [PubMed: 26566717]

56. Pfluger P. T., Kabra D. G., Aichler M., Schriever S. C., Pfuhlmann K., García V. C., Lehti M., Weber J., Kutschke M., Rozman J., Elrod J. W., Hevener A. L., Feuchtinger A., Hrabě de Angelis M., Walch A., Rollmann S. M., Aronow B. J., Müller T. D., Perez-Tilve D., Jastroch M., De Luca M., Molkentin J. D., Tschöp M. H. (2015) Calcineurin links mitochondrial elongation with energy metabolism. *Cell Metab.* 22, 838–850 [PubMed: 26411342]

57. Sciancalepore M., Luin E., Parato G., Ren E., Giniatullin R., Fabbretti E., Lorenzon P. (2012) Reactive oxygen species contribute to the promotion of the ATP-mediated proliferation of mouse skeletal myoblasts. *Free Radic. Biol. Med.* 53, 1392–1398 [PubMed: 22917975]

58. Görlach A., Bertram K., Hudecova S., Krizanova O. (2015) Calcium and ROS: a mutual interplay. *Redox Biol.* 6, 260–271 [PMCID: PMC4556774] [PubMed: 26296072]

59. Gervásio O. L., Whitehead N. P., Yeung E. W., Phillips W. D., Allen D. G. (2008) TRPC1 binds to caveolin-3 and is regulated by Src kinase - role in Duchenne muscular dystrophy. *J. Cell Sci.* 121, 2246–2255 [PubMed: 18544631]

60. Hore P. J., Mouritsen H. (2016) The radical-pair mechanism of magnetoreception. *Annu. Rev. Biophys.* 45, 299–344 [PubMed: 27216936]

61. Usselman R. J., Chavarriaga C., Castello P. R., Procopio M., Ritz T., Dratz E. A., Singel D. J., Martino C. F. (2016) The quantum biology of reactive oxygen species partitioning impacts cellular bioenergetics. *Sci. Rep.* 6, 38543 [PMCID: PMC5172244] [PubMed: 27995996]

62. Kattnig D. R., Evans E. W., Déjean V., Dodson C. A., Wallace M. I., Mackenzie S. R., Timmel C. R., Hore P. J. (2016) Chemical amplification of magnetic field effects relevant to avian magnetoreception. *Nat. Chem.* 8, 384–391 [PubMed: 27001735]

63. Ristow M., Schmeisser K. (2014) Mitohormesis: promoting health and lifespan by increased levels of reactive oxygen species (ROS). *Dose Response* 12, 288–341 [PMCID: PMC4036400] [PubMed: 24910588]

64. Aquilano K., Baldelli S., Pagliei B., Cannata S. M., Rotilio G., Ciriolo M. R. (2013) p53 orchestrates the PGC-1α-mediated antioxidant response upon mild redox and metabolic imbalance. *Antioxid. Redox Signal.* 18, 386–399 [PMCID: PMC3526895] [PubMed: 22861165]

65. Baldelli S., Aquilano K., Ciriolo M. R. (2014) PGC-1α buffers ROS-mediated removal of mitochondria during myogenesis. *Cell Death Dis.* 5, e1515 [PMCID: PMC4260723] [PubMed: 25375380]

66. Sherrard R. M., Morellini N., Jourdan N., El-Esawi M., Arthaut L. D., Niessner C., Rouyer F., Klarsfeld A., Doulazmi M., Witczak J., d'Harlingue A., Mariani J., Mclure I., Martino C. F., Ahmad M. (2018) Low-intensity electromagnetic fields induce human cryptochrome to modulate intracellular reactive oxygen species. *PLoS Biol.* 16, e2006229 [PMCID: PMC6168118] [PubMed: 30278045]

67. Enoki R., Ono D., Kuroda S., Honma S., Honma K. I. (2017) Dual origins of the intracellular circadian calcium rhythm in the suprachiasmatic nucleus. *Sci. Rep.* 7, 41733 [PMCID: PMC5290527] [PubMed: 28155916]

68. Fogle K. J., Baik L. S., Houl J. H., Tran T. T., Roberts L., Dahm N. A., Cao Y., Zhou M., Holmes T. C. (2015) CRYPTOCHROME-mediated phototransduction by modulation of the potassium ion channel β-subunit redox sensor. *Proc. Natl. Acad. Sci. USA* 112, 2245–2250 [PMCID: PMC4343116] [PubMed: 25646452]

69. Jang Y., Lee Y., Kim S. M., Yang Y. D., Jung J., Oh U. (2012) Quantitative analysis of TRP channel genes in mouse organs. *Arch. Pharm. Res.* 35, 1823–1830 [PubMed: 23139135]

70. Tan N., Lansman J. B. (2014) Utrophin regulates modal gating of mechanosensitive ion channels in dystrophic skeletal muscle. *J. Physiol.* 592, 3303–3323 [PMCID: PMC4146377] [PubMed: 24879867]

71. Winegar B. D., Haws C. M., Lansman J. B. (1996) Subconductance block of single mechanosensitive ion channels in skeletal muscle fibers by aminoglycoside antibiotics. *J. Gen. Physiol.* 107, 433–443 [PMCID: PMC2216990] [PubMed: 8868053]

Figures and Tables

Figure 1

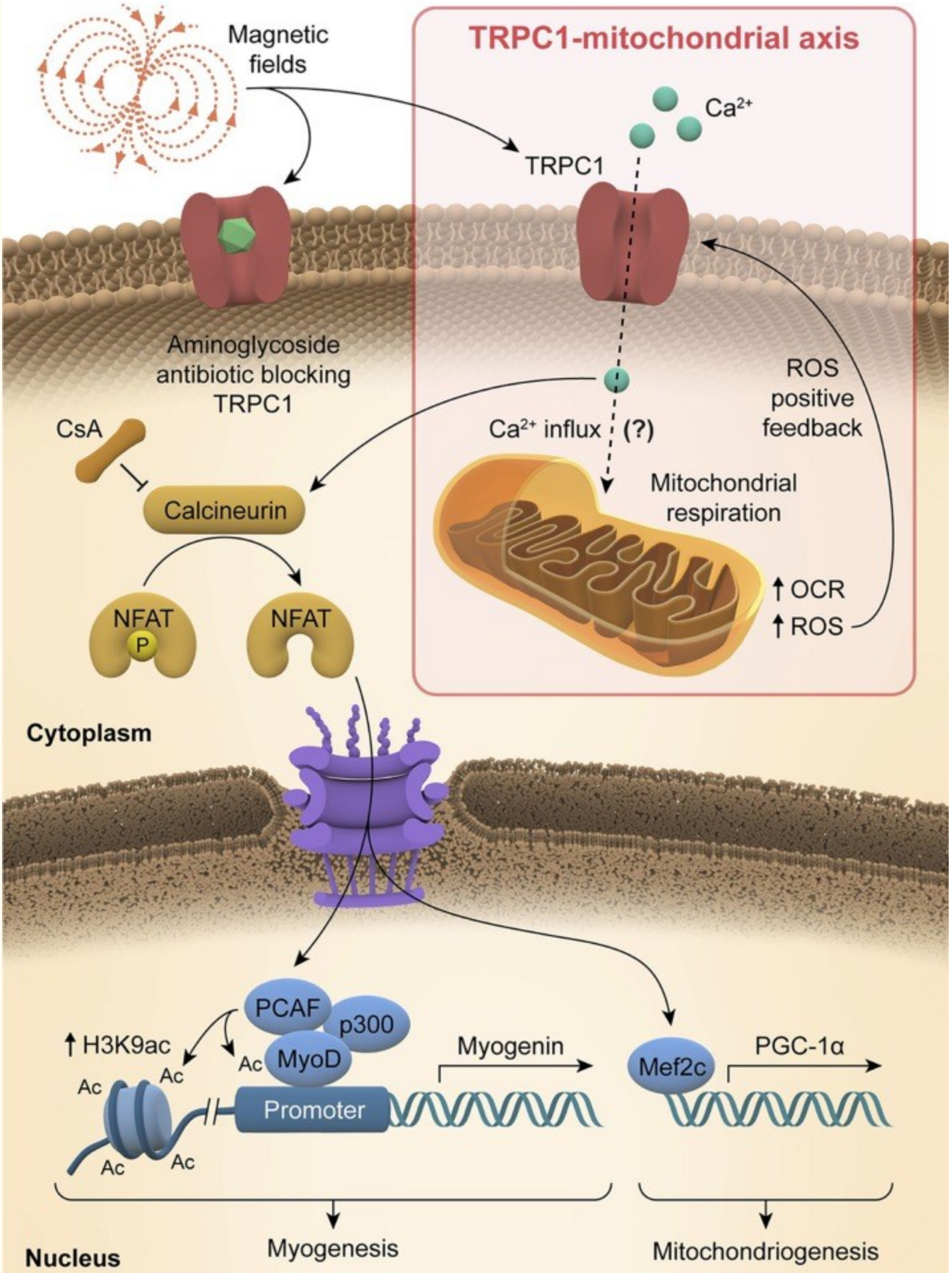
Magnetic fields
TRPC1-mitochondrial axis
Ca2+
TRPC1
Aminoglycoside antibiotic blocking TRPC1
ROS positive feedback
Ca2+ influx (?)
CsA
Calcineurin
Mitochondrial respiration
↑ OCR
↑ ROS
NFAT
P
NFAT
Cytoplasm
PCAF
p300
↑ H3K9ac
Ac
MyoD
Myogenin
Mef2c
PGC-1α
Promoter
Myogenesis
Mitochondriogenesis
Nucleus

Open in a separate window

Graphical abstract. Schematic representation of how magnetic fields activate a TRPC1-mitochondrial axis upstream of calcineurin/NFAT and PCAF genetic and epigenetic pathways, promoting myogenesis and mitochodriogenesis.

TABLE 1

Quantitative PCR primer sets

	Primer sequence, 5′–3′		
Gene	**Forward**	**Reverse**	**Taqman assay ID**
B2M	GATGTCAGATATGTCCTTCAGCA	TCACATGTCTCGATCCCAGT	
PPARGC1A	CCCTGCCATTGTTAAGACC	TGCTGCTGTTCCTGTTTTC	
TERT	ACTCCGTTGTCATCGAGCAG	TGCGTATAGCACCTGTCACC	
MYOD1	ATGGCATGATGGATTACAGCG	TGGAGATGCGCTCCACTATG	
MYOG	CCAACCCAGGAGATCATTTGC	AGTTGGGCATGGTTTCGTCT	
TRPC1	TGGGCCCACTGCAGATTTCAA	AAGATGGCCACGTGCGCTAAGGAG	

	Primer sequence, 5′–3′		
Gene	**Forward**	**Reverse**	**Taqman assay ID**
B2M			Mm00437762_m1
MEF2C			Mm01340842_m1

Figure 2

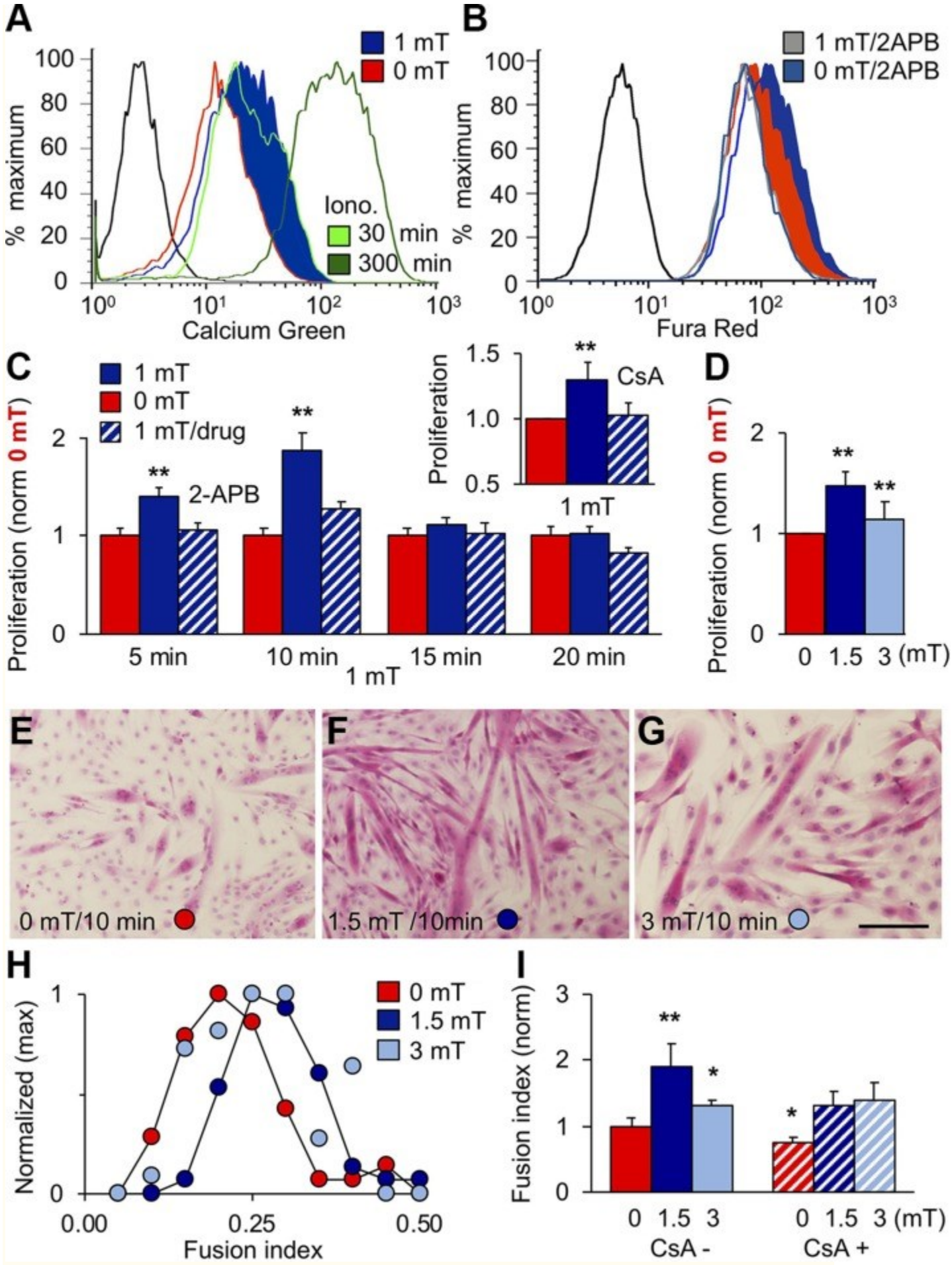
A
1 mT
0 mT
% maximum
Iono.
30 min
300 min
Calcium Green
B
1 mT/2APB
0 mT/2APB
% maximum
Fura Red
C
1 mT
0 mT
1 mT/drug
Proliferation (norm 0 mT)
2-APB
CsA
Proliferation
1 mT
5 min
10 min
15 min
20 min
1 mT
D
Proliferation (norm 0 mT)
0 1.5 3 (mT)
E
0 mT/10 min
F
1.5 mT /10min
G
3 mT/10 min
H
0 mT
1.5 mT
3 mT
Normalized (max)
Fusion index
I
Fusion index (norm)
CsA -
CsA +
0 1.5 3 (mT)

Open in a separate window

PEMF exposure stimulates *in vitro* myogenesis. *A*) $[Ca^{2+}]_i$ following exposures to 0 mT (red), 1 mT (blue), or ionomycin [Iono; 1 μM; 30 (light green) and 300 min (green)] as indicated. *B*) Effect of 2-APB (10 μM) on $[Ca^{2+}]_i$ in response to 0 mT (gray blue) or 1 mT (gray) PEMFs. Unstained cell distributions in black (*A*, *B*). *C*) Effect of PEMF exposure duration on proliferation. Data at each time point were normalized to their own respective control scenario (0 mT) that was treated identically to the experimental condition with the lone exception of no PEMF exposure. 2-APB (light blue) was applied during PEMF exposure. Inset: Effect of CsA (2 μM) on PEMF-induced proliferation; $n = 3$. *D*) PEMF efficacy window (Supplemental Fig. S3). *E–G*) Myotube formation following exposure to 0 (*E*), 1.5 (*F*), or 3 mT (*G*) PEMFs. Scale bar, 500 μm. *H*) Fusion frequency distribution for 0 (red), 1.5 (blue), and 3 mT (light blue) exposures; $n = 3$. *I*) CsA (2 μM) precluded myotube enhancement following 1.5 mT exposure; $n = 10$. All PEMF exposures were applied once <24 h postplating for 10 min, except for *C* as noted; 24 h post-PEMF exposure myoblasts were either counted (*C*, *D*) or allowed to differentiate (*E–I*) for 6 d. $^*P < 0.05$, $^{**}P < 0.01$ (with regard to 0 mT).

Figure 3

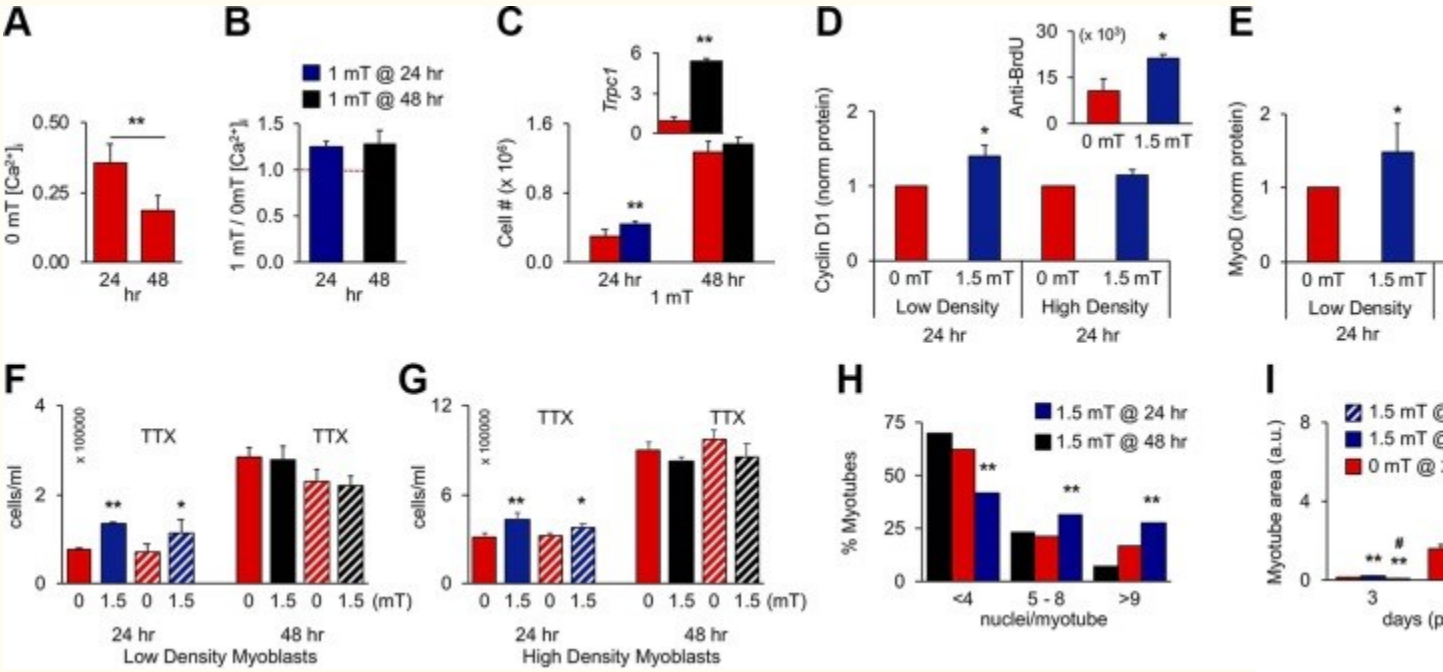

PEMF exposure enhances *in vitro* myogenesis when applied once before 24 h postplating. *A*) Resting $[Ca^{2+}]_i$ at 24 or 48 h in culture; $n = 4$. *B*) PEMF-induced $[Ca^{2+}]_i$ at 24 or 48 h; $n = 4$. Despite resting $[Ca^{2+}]_i$ being depressed at 48 h (*A*), PEMFs remained capable of augmenting $[Ca^{2+}]_i$ (*B*), indicating that TRPC1-mediated calcium entry was operational, albeit down-regulated at 48 h. *C*) Proliferative responses to 1 mT exposure at 24 or 48 h; $n = 8$ (inset: despite the absence of proliferative response at 48 h, *Trpc1* transcript levels rose 1 h after exposure). *D*, *E*) Cyclin D1 (*D*) and MyoD (*E*) protein levels following PEMF exposure at 24 h on low-density (~2500 cells/cm^2) or high-density (~8500 cells/cm^2) cultures; $n = 3$ or 5, respectively. Protein was collected 24 h after PEMF exposure as indicated. Inset: anti-BrdU-FITC positive myoblasts 6 h after PEMF exposure. *F*, *G*) Effects of TTX (1 μM) on PEMF-mediated proliferation applied at 24 and 48 h, as indicated, in low-density (*F*) or high-density (*G*) myoblast cultures. *H*) Nuclei/myotube distribution for exposures to 1.5 mT at 24 (blue) or 48 h (black); 0 mT (red). $^*P < 0.05$, $^{**}P < 0.01$ (with regard to 0 mT, respectively) (*A–G*). *I*) Effect of repeated stimulation on differentiation on myoblast cultures exposed once (blue; 24 h) or consecutively for 4 d

(hatched). Myoblasts cultures were exposed at the indicated times and then either analyzed for proliferation/calcium entry (*A–G*) or induced to differentiate for subsequent analysis (*H–I*). $^{**}P < 0.01$, $^{\#}P < 0.05$ with regard to 0 or 1.5 mT, respectively (*I*). All PEMF exposures were 10 min.

Figure 4

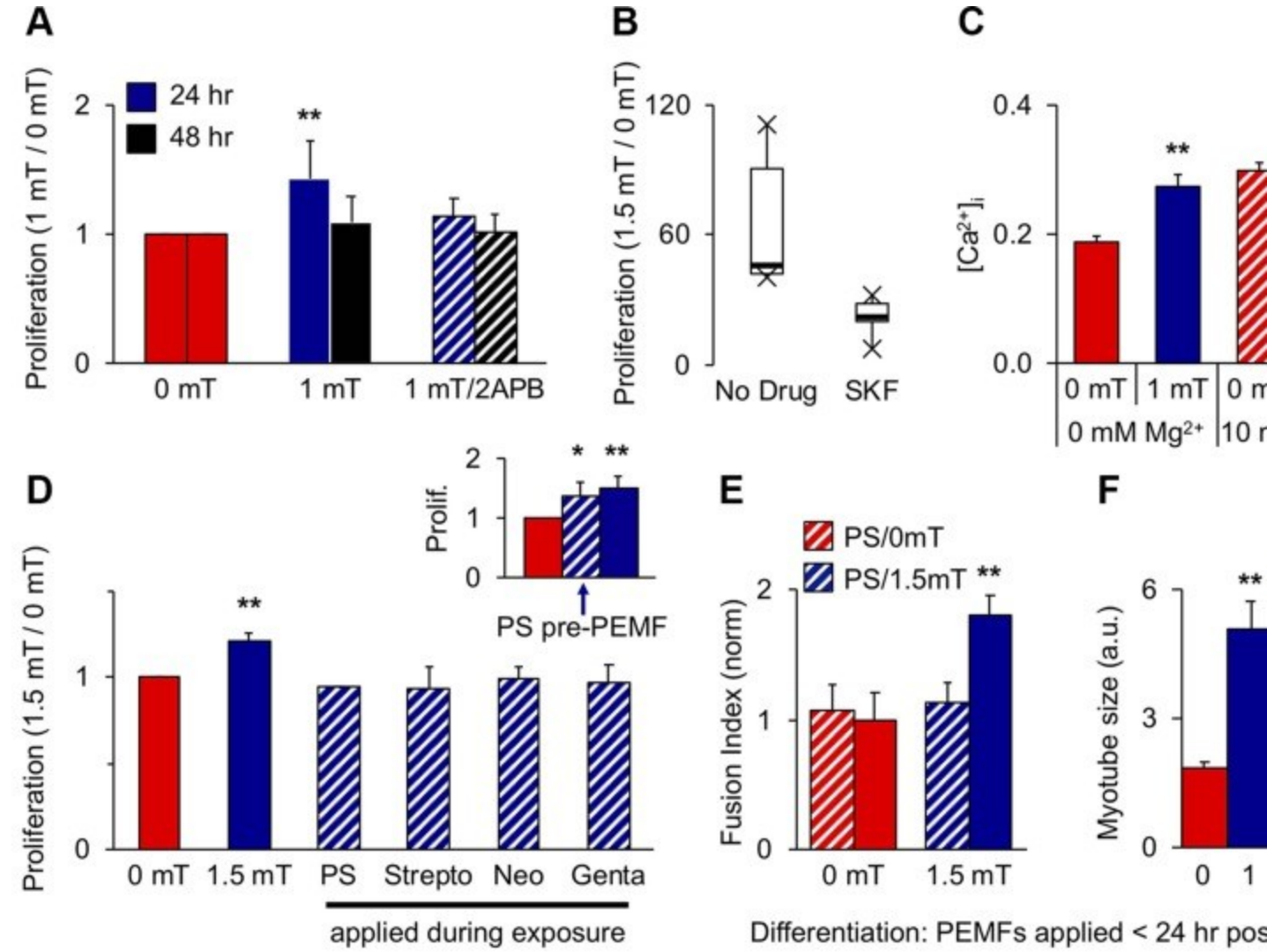
A
Proliferation (1 mT / 0 mT)
24 hr
48 hr
**
0 mT
1 mT
1 mT/2APB
B
Proliferation (1.5 mT / 0 mT)
No Drug
SKF
C
[Ca2+]i
**
0 mT
1 mT
0 mM Mg2+
D
Proliferation (1.5 mT / 0 mT)
**
Prolif.
* **
PS pre-PEMF
0 mT
1.5 mT
PS
Strepto
Neo
Genta
applied during exposure
E
PS/0mT
PS/1.5mT **
Fusion Index (norm)
0 mT
1.5 mT
F
Myotube size (a.u.)
**
Differentiation: PEMFs applied < 24 hr pos

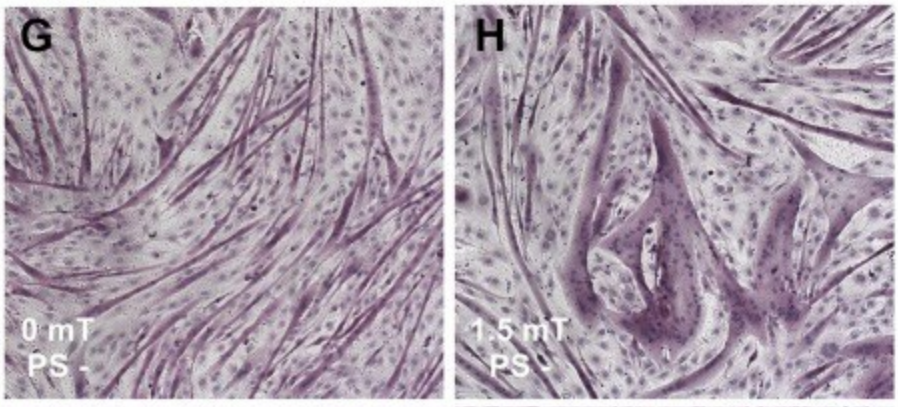
G
0 mT
PS -
H
1.5 mT
PS -
J
0 mT
PS +
K
1.5 mT
PS +

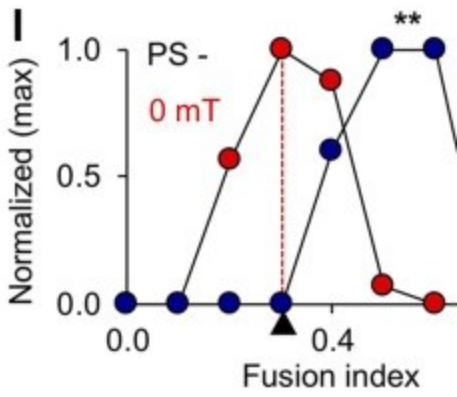
I
Normalized (max)
PS -
0 mT
**
Fusion index
L
PS +
0 mT
1.5 mT

Pharmacological evidence implicating TRPC1 in magnetoreception. *A*) Effect of 2-APB (10 µM; hatched) on PEMF-induced proliferation at 24 h (dark blue) and 48 h (black) after plating; $n = 11$ (24 h) and $n = 7$ (48 h). *B*) Effect of SKF-96365 (50 µM) on PEMF-induced proliferation; $n = 5$. *C*) Levels of $[Ca^{2+}]_i$ following 10 min exposure to 0 (red) or 1 mT (blue) PEMFs in the absence (solid) or presence (hatched) of 10 mM $MgCl_2$ (hexahydrate) added to the culture medium immediately before exposure; $n = 3 \pm$ SEM). *D*) PEMF-modulated proliferation (Prolif; 1.5/0 mT) in response to no antibiotics (solid), penicillin/streptomycin (PS) (1%, hatched), streptomycin (Strepto; 100 mg/L), neomycin (Neo; 50 mg/L), or gentamycin (Genta; 50 mg/L) added to the culture medium at time of PEMF exposure; $n = 4$. Inset: effect of 10 min PS application and immediate removal 2 h before PEMF exposure; $n = 3$. *E*, *F*) PS (1%) (*E*) and Neo (50 mg/L) (*F*) prevented myotube formation following single PEMF exposure. *G–L*) Myotube formation without (*G–I*) and with (*J–L*) PS (1%) as indicated. Scale bar, 100 µm. *M*) PS and 2-APB attenuate 2-APB–sensitive PEMF-induced calcium entry; $n = 2 \times 8$ wells. *N*, *O*) Myotube size distribution without (*N*) and with (*O*) CsA; correspondent to Fig. 2*I*. The red dashed lines indicate the previous 0 mT level. Unless otherwise stated, all data are generated from the means of independent experiments ± SD each pertaining to minimally the means of biological triplicates. All PEMF exposures were conducted for 10 min applied 24 h postplating, unless otherwise stated (48 h; *A*); 24 h post-PEMF exposure myoblasts were either counted (*B–D*) or allowed to differentiate (*E*, *F*) for 6 d. $^{**}P < 0.01$ (with regard to 0 and 1.5 mT, black and red asterisks, respectively). All drugs were applied transiently to coincide with PEMF exposure and to avoid non-TRP channel–related tertiary effects. Specifically, 2-APB, SKF-96365, and antibiotics were added to culture medium before PEMF exposure and then replaced with age-matched control medium from sister cultures summarily thereafter, with the exception of *D* (inset), wherein PS (hatched) was added and removed before PEMF exposure.

Figure 5

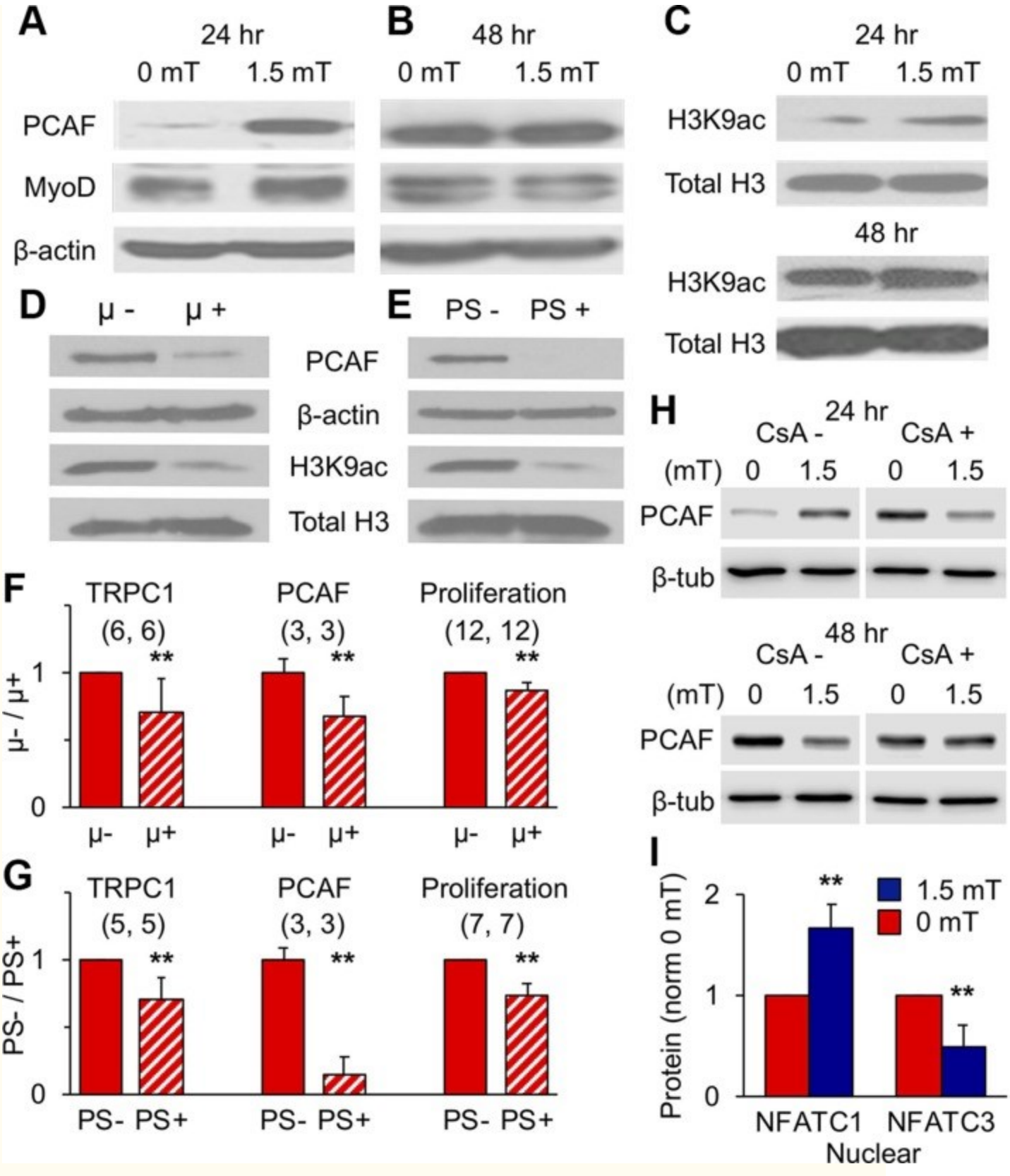
A
24 hr
0 mT
1.5 mT
PCAF
MyoD
β-actin
B
48 hr
0 mT
1.5 mT
C
24 hr
0 mT
1.5 mT
H3K9ac
Total H3
48 hr
H3K9ac
Total H3
D
μ -
μ +
PCAF
β-actin
H3K9ac
Total H3
E
PS -
PS +
H
24 hr
CsA -
CsA +
(mT) 0 1.5 0 1.5
PCAF
β-tub
48 hr
CsA -
CsA +
(mT) 0 1.5 0 1.5
PCAF
β-tub
F
TRPC1
(6, 6)
PCAF
(3, 3)
Proliferation
(12, 12)
**
μ- / μ+
1
0
μ- μ+
μ- μ+
μ- μ+
G
TRPC1
(5, 5)
PCAF
(3, 3)
Proliferation
(7, 7)
**
PS- / PS+
1
0
PS- PS+
PS- PS+
PS- PS+
I
**
1.5 mT
0 mT
Protein (norm 0 mT)
2
1
0
**
NFATC1
NFATC3
Nuclear

Magnetic fields promote epigenetic MyoD. *A*, *B*) PEMF-modulated PCAF and MyoD protein levels at 24 (*A*) or 48 (*B*) h postplating. *C*) H3K9 histone acetylation levels after 1.5 mT PEMF exposure at 24 (top) or 48 (bottom) h postplating. *D*, *E*) PCAF protein and H3K9 acetylation levels after growth of myoblasts within a μ-metal box (*D*) or in the presence of PS (PS; 1%; for 72 h (*E*). *F*, *G*) Protein levels of TRPC1 and PCAF and proliferation after 72-h growth in a μ-metal box (*F*, μ^+) or in the presence of PS (*G*, PS+) relative to controls (μ−, PS−); (*n*/condition). *H*) Effects of CsA (2 μM) over PEMF-modulated PCAF expression at 24 or 48 h. *I*) Nuclear and cytoplasmic distribution of NFATC1 and NFATC3 following 1.5 mT exposure (blue) at 25 h postplating (see also Supplemental Fig. S8); $n = 6$/condition. Data represent the means of *n* experiments ± SD), each derived from the means of triplicates. All PEMF exposures were 10 min. $^{**}P < 0.01$ with regard to relative control.

Figure 6

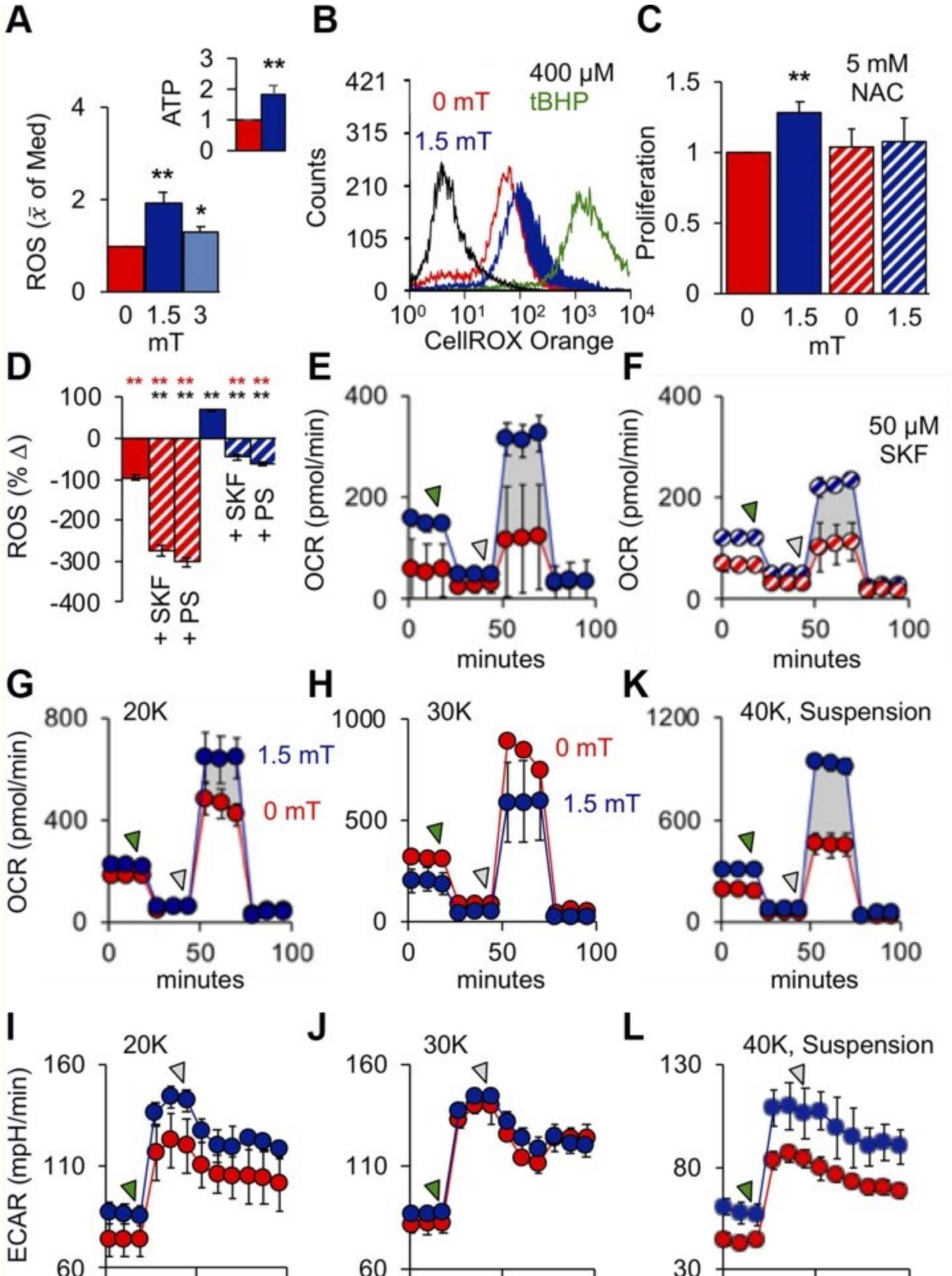
A
ROS ($\bar{x}$ of Med)
ATP
mT
B
400 µM
tBHP
0 mT
1.5 mT
Counts
CellROX Orange
C
5 mM
NAC
Proliferation
mT
D
ROS (% Δ)
+ SKF
+ PS
E
OCR (pmol/min)
minutes
F
50 µM
SKF
G
20K
1.5 mT
0 mT
H
30K
K
40K, Suspension
I
ECAR (mpH/min)
J
L

Open in a separate window

PEMFs activate mitochondrial respiration upstream of myogenic enhancement. *A*) ROS (H_2O_2) production in response to PEMF exposure and normalized to that at 0 mT; $n = 6$. Inset: SKF-inhabitable ATP production 30 min following PEMF exposure (10 min at 1.5 mT); $n = 3$. *B*) ROS production in response to exposure to PEMFs or 400 μM tert-butyl hydroperoxide (tBHP; 1 h; green). *C*) Normalized proliferation (relative 0 mT) in response to PEMF exposure with and without *N*-acetylcysteine (NAC); $n = 9$. *D*) Percentage change in ROS production immediately after PEMF exposure with and without PS (PS; 1%) or SKF-96365 (SKF; 50 μM). Data shown indicate ROS quantification 6–8 min after reading commenced. *E*, *F*) Mitochondrial OCR in response to PEMF exposure without (*E*) and with (*F*) SKF-96365. *G–J*) OCR and ECAR in myoblasts plated at 20,000 (*G* and *I*, respectively) and 30,000 (*H* and *J*, respectively) per well. *K*, *L*) OCR (*K*) and ECAR (*L*) in myoblasts exposed to PEMFs in suspension and then plated at 40,000 myoblasts/well 5 h before measurement. The green- and gray-shaded arrows indicate points of addition of oligomycin (ATP synthase inhibitor; 1 μM) and carbonyl cyanide 4-(trifluoromethoxy) phenylhydrazone (mitochondrial proton ionophore; 1 μM), respectively. Unless otherwise stated, all PEMF exposures (blue) was applied for a duration of 10 min at an amplitude of 1.5 mT with (hatched) or without (solid) drugs as indicated; red represents correspondent control scenarios. $^{**}P < 0.01$ with regard to correspondent 0 and 1.5 mT scenarios, respectively.

TABLE 2

Mitochondrial respiratory parameters (1.5/0 mT)

Exposure condition	Basal respiration	*P*	Spare capacity	*P*	ATP production	*P*
C2C12 wild type						
20 K (plated; $n = 9$)	1.13 ± 0.15	0.0228[a]	1.25 ± 0.25	0.0104[a]	1.12 ± 0.12	0.0115[a]
30 K (plated; $n = 5$)	0.91 ± 0.13	0.1207[a]	0.89 ± 0.11	0.0608[a]	0.96 ± 0.12	0.2671[a]
		0.0142[b]		0.0075[b]		0.02370[b]

Exposure condition	Basal respiration	*P*	Spare capacity	*P*	ATP production	*P*
40 K (suspension-low ρ; *n* = 4)	1.64 ± 0.29	0.0041[a]	1.95 ± 0.48	0.0071[a]	1.67 ± 0.31	0.0052[a]
40 K (suspension-high ρ; *n* = 4)	0.91 ± 0.08	0.0694[a]	0.88 ± 0.09	0.0499[a]	0.92 ± 0.01	0.0895[a]
		0.0053[c]		0.0091[c]		0.0071[c]
24 h (*n* = 2)	1.35 ± 0.08		1.54 ± 0.31		1.29 ± 0.12	
48 h (*n* = 2)	1.09 ± 0.05		1.12 ± 0.17		1.11 ± 0.03	
CRISPR/Cas9 TRPC1 knockdown						
c60 (*n* = 4)	0.97 ± 0.14	0.6768[a]	0.87 ± 0.24	0.3759[a]	0.95 ± 0.15	0.5628[a]
c61 (*n* = 4)	0.95 ± 0.05	0.0582[a]	0.90 ± 0.07	0.0462[a]	0.93 ± 0.05	0.0482[a]

Exposure condition	Basal respiration	*P*	Spare capacity	*P*	ATP production	*P*
		0.3769[d]		0.4104[d]		0.4338[d]

All values represent means ± SD of *n* independent experiments. “Suspension-low ρ” and “suspension-high ρ” refer to myoblast suspensions originating from either low- or high-density cultures, respectively, before exposure to PEMFs as indicated and then plated at 40,000 myoblasts/well 6 h before mitochondrial respiratory assessment. *P* values indicate: [a]0 mT with regard to 1.5 mT; [b]20 K with regard to 30 K; [c]low ρ with regard to high ρ; [d]c60 with regard to c61.

Figure 7

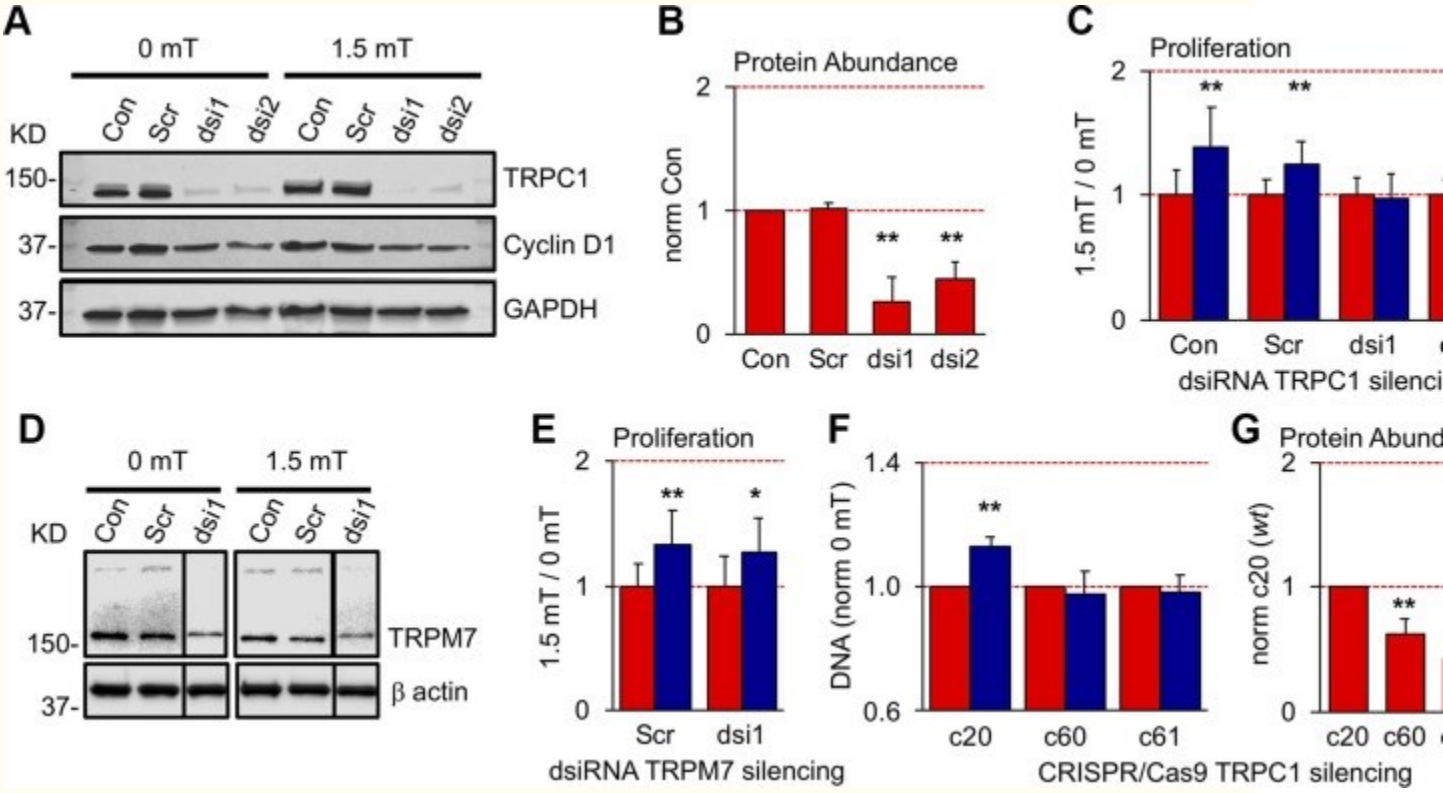

TRPC1 silencing precludes PEMF sensitivity. *A*) Western blots showing protein levels of TRPC1 and cyclin D1 following transfection with targeted (dsi1 and dsi2) and nontargeted Scr dsiRNAs. TRPC1 silencing decreased basal cyclin D1 levels by ~10%, whereas PEMF exposure increased cyclin D1 levels by 15% in controls (Con, Scr), compared with negligible PEMF-induced changes in TRPC1-silenced myoblasts, dsi1 (3%) and dsi2 (−5%). *B*) Normalized protein abundance of TRPC1 relative to Con. *C*) Proliferative responses of TRPC1-silenced and Con myoblasts to PEMF exposure (blue, 1.5 mT) relative to unexposed (0 mT; red); *n* = 6. *D*) TRPM7 protein abundance following silencing using 1 dsiRNA (dsi1). The data (lane) from another ineffective dsiRNA was removed for clarity and is delineated by the black border. *E*) TRPM7-silenced (ds1) and nonsilenced (Scr) myoblasts exhibited normal PEMF-

induced proliferative enhancements; $n = 6$. *F*) Cellular DNA content, reflecting cell number, following PEMF exposure in CRISPR/Cas9 TRPC1-silenced clones, c60 and c61, relative to wild-type clone, c20. *G*) CRISPR/Cas9 targeted deletion of TRPC1 exon 1 reduced TRPC1 expression by ~40 and 60% in clones c60 and c61, respectively, relative to wild-type clone, c20. See Supplemental Fig. S9 for details of the CRISPR/Cas9 deletion of TRPC1 exon 1; $n = 3$. All PEMF exposures were for 10 min. *$P < 0.05$, **$P < 0.01$ (with regard to correspondent 0 mT or Con scenario).

Figure 8

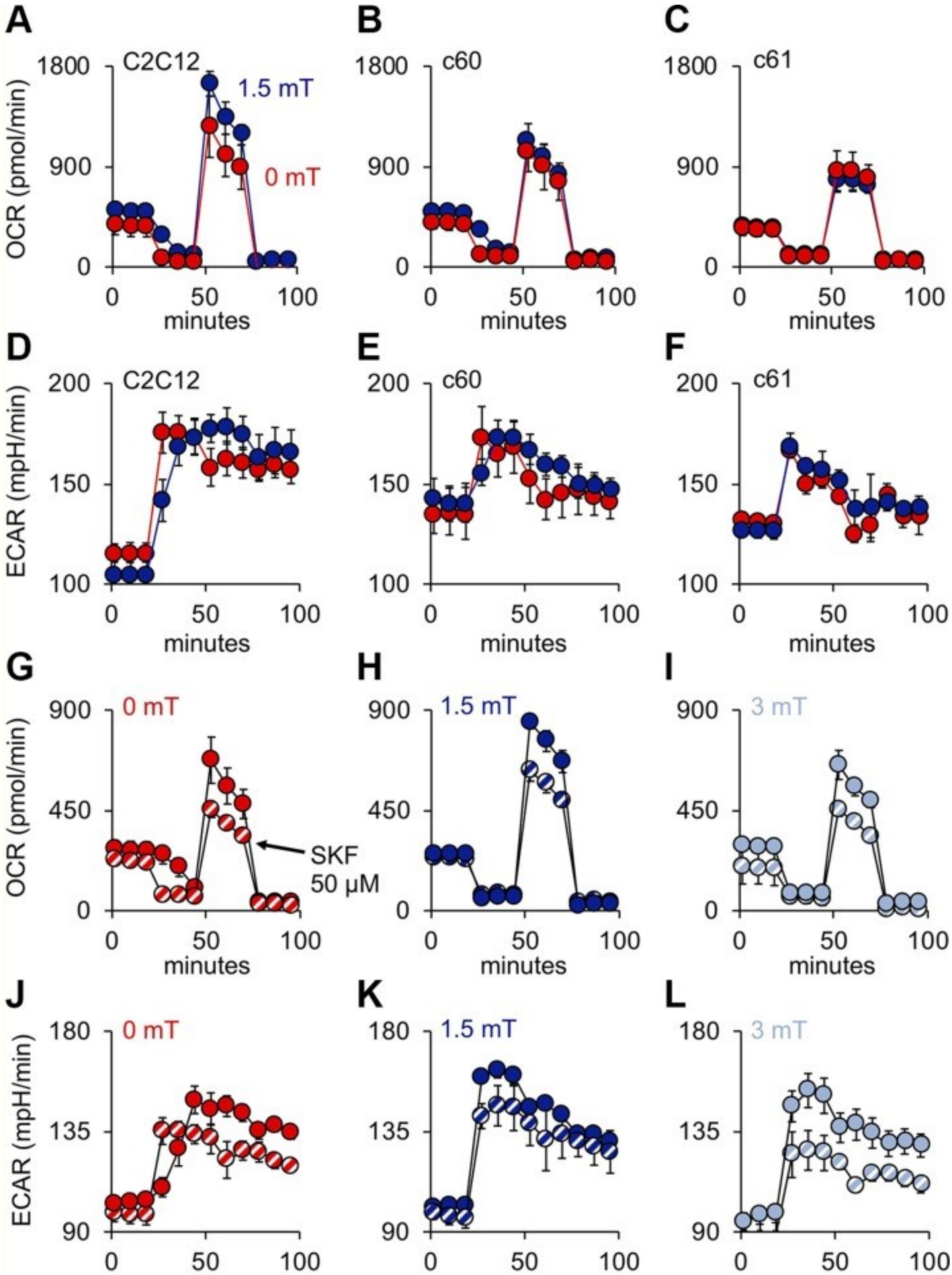
A
B
C
C2C12
c60
c61
1.5 mT
0 mT
OCR (pmol/min)
1800
900
0
0
50
100
minutes
D
E
F
ECAR (mpH/min)
200
150
100
G
H
I
3 mT
SKF
50 μM
J
K
L
180
135
90

Mitochondrial oxidative capacity parallels TRPC1 channel expression and magnetic sensitivity. *A–C*) Mitochondrial OCR in response to PEMF exposure in wild-type C2C12 myoblasts (*A*) and in CRISPR/Cas9 TRPC1-silenced clones c60 (*B*) and c61 (*C*) (also see Table 2). *D–F*) ECAR in wild-type C2C12 myoblasts (*D*) and in CRISPR/Cas9 TRPC1-silenced clones c60 (*E*) and c61 (*F*). *G–I*) Mitochondrial OCR from wild-type C2C12 myoblasts in response to 10 min exposures to 0 (*G*), 1.5 (*H*), or 3 mT (*I*) amplitude PEMFs in the absence (solid symbols) or presence (hatched symbols) of SKF-96365 (SKF; 50 μM) as indicated. *J–L*) ECAR in wild-type C2C12 myoblasts in response to 10 min exposures to 0 (*J*), 1.5 (*K*), or 3 mT (*L*) amplitude PEMFs in the absence (solid symbols) or presence (hatched symbols) of SKF (50 μM) as indicated.

Figure 9

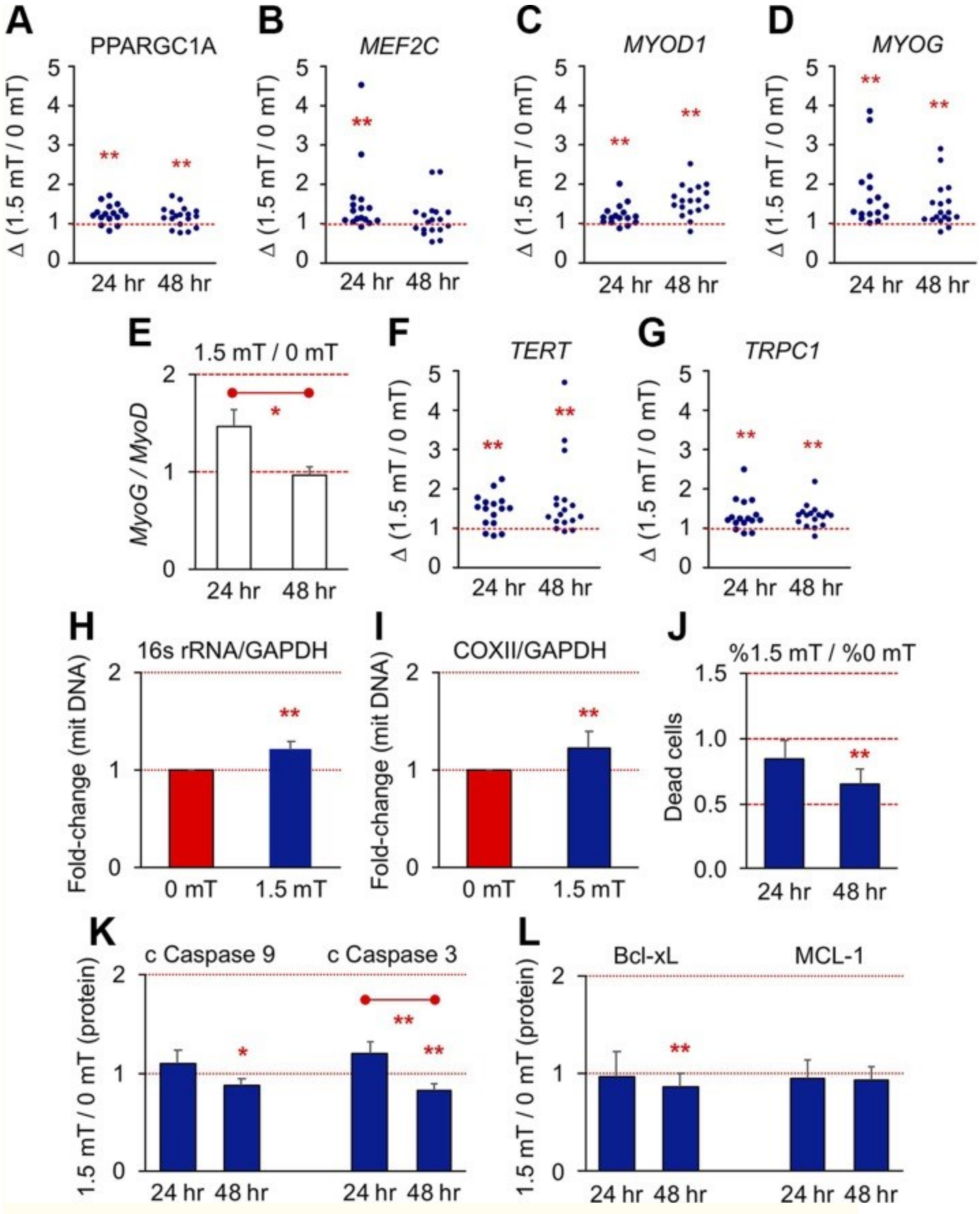
A
PPARGC1A
B
MEF2C
C
MYOD1
D
MYOG
Δ (1.5 mT / 0 mT)
24 hr 48 hr
E
1.5 mT / 0 mT
MyoG / MyoD
F
TERT
G
TRPC1
H
16s rRNA/GAPDH
Fold-change (mit DNA)
0 mT 1.5 mT
I
COXII/GAPDH
J
%1.5 mT / %0 mT
Dead cells
K
c Caspase 9
c Caspase 3
1.5 mT / 0 mT (protein)
L
Bcl-xL
MCL-1

PEMFs promote mitochondriogenesis and functional adaptations. *A–D*, *F*, *G*) Gene expression scatter plots at 24 and 48 h post-PEMF treatment for the indicated genes. *E*) Myogenin (MyoG) to MyoD ratio at 24 and 48 h following PEMF exposure. For gene expression at early time points, the highest value at 16 or 24 h was taken. Also see **Table 3**. *H*, *I*) Change in mitochondrial DNA relative to nuclear DNA 24 h post-PEMF for 16s rRNA/GAPDH (*H*) and cytochrome c oxidase subunit II (COXII)/GAPDH (*I*); $n = 6 \pm$ SD. *J*) Differential percentage of Trypan Blue positive (dead) cells after 24 and 48 h post-PEMF exposure; $n = 7 \pm$ SEM). *K*, *L*) Proapoptotic (*K*) and antiapoptotic (*L*) protein expression at 24 and 48 h post-PEMF exposure as indicated; $n = 12 \pm$ SEM. $^{*}P < 0.05$, $^{**}P < 0.01$ (with regard to correspondent 0 mT control scenario or as indicated by bar). All data represent the mean of *n* independent experiments each pertaining to the means of biological triplicates.

TABLE 3

Quantification of gene expression

Gene	24 h	48 h
PPARGC1A	1.25 ± 0.23 (*n* = 16)	1.18 ± 0.25 (*n* = 18)
MEF2C	1.55 ± 0.88 (*n* = 16)	1.14 ± 0.48 (*n* = 18)
MYOD1	1.22 ± 0.26 (*n* = 16)	1.58 ± 0.39 (*n* = 18)
MYOG	1.74 ± 0.83 (*n* = 16)	1.45 ± 0.55 (*n* = 18)
TERT	1.45 ± 0.41 (*n* = 16)	1.73 ± 0.97 (*n* = 17)
TRPC1	1.34 ± 0.39 (*n* = 16)	1.32 ± 0.29 (*n* = 17)
MYOG/MYOD1	1.46 ± 0.71 (*n* = 16)	0.96 ± 0.38 (*n* = 17)

Each value represents the mean ± SD. Significance is indicated in Fig. 9*A*–*G*; *n* is the number of individual PCR reactions from 9 different samples run on different dates.

Figure 10

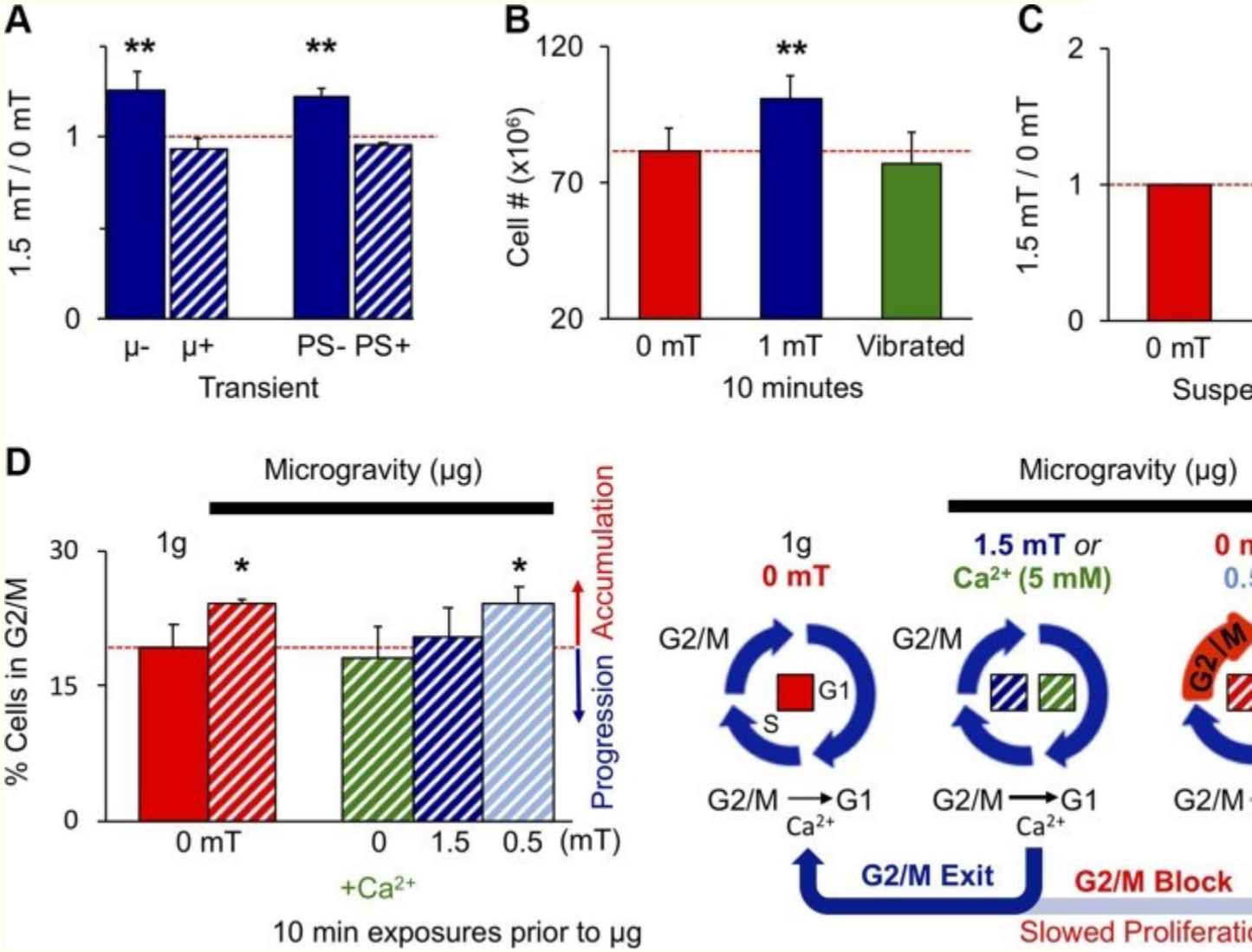

Evidence for magnetic specificity. *A*) Coincident μ-metal shielding or PS administered only during PEMFs exposure precluded proliferative response (Supplemental Fig. S1*C*); *n* = 6. *B*) Vibrating myoblasts at the same frequency and amplitude as they experience during PEMF exposure does not recapitulate the proliferative effects of PEMF exposure relative to nonvibrated, nonexposed myoblasts (red); *n* = 4. *C*) Exposing myoblasts to PEMFs while in suspension did not preclude a proliferative response; *n* = 4. *D*) PEMF exposure (1.5 mT; dark blue hatched) or 5 mM $CaCl_2$ (green hatched) applied to C2C12 cultures for 10 min before placement into simulated microgravity (hatched) transiently rescued G_2/M accumulation of myoblasts caused by gravitational mechanical unloading (μ*g*; red hatched) (12), whereas 0.5 mT PEMFs (light blue hatched) did not; *n* = 3. All data are generated from the means of independent experiments ± SD each pertaining to minimally the means of triplicates. All PEMF exposures were for 10 min. $^{**}P < 0.01$, $^{*}P < 0.05$ [with regard to correspondent control scenarios (0 mT)].